P. 56

NASA Technical Memorandum 100660

IN-34
310414
DATE OVERRIDE

MEASURED AND PREDICTED SHOCK SHAPES FOR AFE CONFIGURATION AT MACH 6 IN AIR AND IN CF_4

(NASA-TM-100660) MEASURED AND PREDICTED SHOCK SHAPES FOR AFE CONFIGURATION AT MACH 6 IN AIR AND IN CF4 (NASA) 56 p CSCL 20D

N91-10245

Unclas

G3/34 0310414

William L. Wells

Alan M. Franks

October 1988

Date for general release October 31, 1990

National Aeronautics and Space Administration

Langley Research Center
Hampton, Virginia 23665-5225

MEASURED AND PREDICTED SHOCK SHAPES FOR AFE CONFIGURATION AT MACH 6 IN AIR AND IN CF_4

William L. Wells and Alan M. Franks

SUMMARY

Shock shapes and stand-off distances were obtained for the Aeroassist Flight Experiment configuration from Mach 6 tests in air and in CF_4. Results were plotted for an angle-of-attack range from -10° to 10° and comparisons were made at selected angles with inviscid-flow predictions. Tests were performed in the LaRC 20-Inch Mach 6 Tunnel (air) at unit free-stream Reynolds numbers ($N_{Re,\infty}$) of 2 x 10^6/ft and 0.6 x 10^6/ft and in the LaRC Hypersonic CF_4 Tunnel at $N_{Re,\infty}$ = 0.5 x 10^6/ft and 0.3 x 10^6/ft. Within the range of these tests, $N_{Re,\infty}$ did not affect the shock shape or stand off distance, and the predictions were in good agreement with the measurements. The shock stand-off distance in CF_4 was approximately one-half that in air. This effect resulted from the difference in density ratio across the normal shock, which was approximately 12 in CF_4 and 5 in air. In both test gases, the shock lay progressively closer to the body as angle of attack decreased.

SYMBOLS

E	exponential factor (E + 06 = 10^6)
L	diameter of forebody base in symmetry plane
M	Mach number
N_{Re}	unit Reynolds number, 1/ft
p	pressure, psi
q	dynamic pressure, psi
T	temperature, degrees Rankine
X	axis normal to forebody base

Y	axis parallel to forebody base in symmetry plane
Z	axis through elliptic cone apex (see fig. 1)
α	angle of attack with respect to Z axis (see fig. 1), degrees
γ	ratio of specific heats of test gas
δ	cone rake angle in figure 1(a), degrees
θ	elliptic cone half-angle in symmetry plane (see fig. 1), degrees
ρ	density of test gas, lbm/ft^3

Subscripts

1 or ∞	free-stream conditions
2	post shock conditions
t	stagnation conditions

INTRODUCTION

Upon return from high-Earth orbit (e.g., geosynchronous orbit), aero-assisted orbital transfer vehicles (AOTV's) proposed for the 1990's and beyond will use the Earth's atmosphere to decrease their velocity sufficiently to allow insertion into low-Earth orbit, e.g., Space Station orbit (ref. 1.). The high-velocity, high-altitude trajectory of these low-lift, high-drag vehicles will be mostly outside the range of previous flight experience. To help develop a data base for AOTV design, a flight experiment has been proposed primarily because present test facilities are, for the most part, unable to duplicate or simulate this high-velocity, low-density flow environment (ref. 2). The Aeroassist Flight Experiment (AFE) will provide an experimental data base for validation and refinement of current computational fluid dynamic (CFD) codes to be used in future AOTV designs. However, the AFE

itself requires a data base for an accurate determination of aerodynamic and aerothermodynamic flight characteristics, and present test facilities, in conjunction with the best-available CFD codes, must provide this information. A preflight test program in ground-based facilities has been initiated (Ref. 3), and the shock shapes presented in this paper are a part of the results obtained in that program to date.

AEROASSIST FLIGHT EXPERIMENT

The basic AFE flight vehicle will be composed of a 14-foot-diameter drag brake, an instrument compartment or payload at the base, a solid rocket propulsion motor, and small control motors. The vehicle will be carried to low-Earth orbit by the Space Shuttle Orbiter. A solid rocket motor will propel the vehicle into the atmosphere at velocities corresponding to a return from geosynchronous orbit, and onboard guidance, navigation, and control will allow a sweep through the atmosphere and subsequent recovery of the vehicle by the Space Shuttle Orbiter. Approximately a dozen onboard experiments will gather information during the flight to provide a better understanding of the flow environment at these high-altitude, high-velocity entry conditions (Ref. 4).

The basic shape of the AFE drag brake is a 60° (1/2-angle) elliptically blunted right elliptic cone (fig. 1). To provide the desired lift-to-drag value of about 0.3, the base is raked off at an angle $\delta = 73°$. According to modified Newtonian theory, this configuration will trim at an angle of attack of zero with respect to the cone axis and will be statically stable about the center of the rake plane (ref. 5). To reduce heating in the nose region, the cone apex is replaced with an ellipsoid; to reduce heating at the shoulder a

toroid-section skirt provides a rounded shoulder at the base periphery. A detailed analytical description of the configuration is presented in reference 6.

WIND TUNNELS

Langley 20-Inch Mach 6 Tunnel

The 20-Inch Mach 6 Tunnel is a blowdown wind tunnel that uses dry air as the test gas. The air is heated to a maximum temperature of approximately 1100°R by an electrical resistance heater; the maximum reservoir pressure is 525 psia. A fixed geometry, two-dimensional contoured nozzle with parallel side walls expands the flow to Mach 6 at the 20-inch square test section. Two 16.5-inch-diameter clear tempered glass windows are located on opposite sides of the test section. A vertical reference line is located at one window for verification of angle of attack in schlieren photographs. A description of this facility and calibration results are presented in reference 7. Nominal flow conditions for the present tests are shown in Table I.

Langley Hypersonic CF_4 Tunnel

The Hypersonic CF_4 Tunnel is a blowdown wind tunnel that uses tetra-fluoromethane (CF_4) test gas which has a ratio of specific heats that is approximately 20 percent lower than air. The CF_4 is heated to a maximum temperature of 1530°R by two molten lead-bath heat exchangers connected in parallel. The maximum pressure in the tunnel reservoir is 2600 psia. Flow is expanded through an axisymmetric, contoured nozzle designed to generate a Mach number of 6 at the 20-inch-diameter exit. This facility has an open jet test section with two 24-inch by 30-inch clear tempered glass windows on opposite sides. A vertical reference line is located at one window for verification

of angle of attack in schlieren photographs. A detailed description of the CF_4 tunnel and recent calibration results are presented in reference 8. Nominal flow conditions for the present tests are shown in Table II.

WIND TUNNEL MODELS

Schlieren photographs were taken during tests that utilized models designed for pressure and aerodynamic force measurements. Three models were involved in the tests, two force models and one pressure model. One force model and the pressure model were 3.67 inches in diameter, and the second force model was 2.50 inches in diameter. The forebody configuration was the same on all models, but the afterbody of the pressure model was different from the force models. The afterbodies which are centered on the forebody leeside are completely hidden from the oncoming flow, however, and should not influence the shape of the bow shock. Photographs of the pressure and force models are shown in figure 2. (Pressure orifices are on the side opposite to that shown.)

INSTRUMENTATION

To obtain the schlieren photographs, z-type mirror systems were used in both test facilities, with the knife edges mounted parallel to the test section flow direction. In the CF_4 tunnel, the images were recorded on 4-inch by 5-inch black-and-white film, and the exposure time corresponded to the 8-μsec pulse length of the zenon light source. In the air tunnel, the images were recorded on 70-mm black-and-white film, and the exposure time corresponded to the 1-μsec flash of light in a spark gap. All film was developed and enlarged to 8-inch by 10-inch prints. Typical schlieren photographs are shown in figure 3.

PREDICTION METHOD

HALIS is an acronym for the High Alpha Inviscid Solution computer code (ref. 9). The HALIS code is a time-asymptotic solution of the Euler equations where the solution space is the volume between the body surface and the bow shock which is treated as a time dependent boundary. The code will handle arbitrary perfect gases (constant ratio of specific heats) or real gases in thermodynamic equilibrium. To avoid numerical instabilities around the aft corner of the AFE configuration, a cylindrical extension downstream of the forebody was incorporated in the numerical model. The cylindrical extension is parallel to the Z axis (fig. 1) and is tangent to the aft corner of the forebody; otherwise the numerical and physical (wind tunnel) models are the same (fig. 4). In the present study, free-stream flow conditions were used as inputs to the code, and properties for CF_4 were calculated from the relations of reference 10. The predictions included herein were furnished by J. K. Weilmuenster of the Langley Research Center.

DIGITIZING PROCESS

The shock shapes were obtained from 8- x 10-inch black-and-white schlieren photographs. Each photograph was mounted on a plotter so that the AFE base was vertical as required by the digitizing program. To account for variations in photographs or model size, the model base diameter was measured from each photograph and entered into the digitizing program for use as a reference length. With a photograph fixed in position, the plotter, equipped with an optical sight device, was used to locate and record the geometric stagnation point (intersection of Z axis with front surface in fig. 1) on the model which was defined as the origin of the X-Y coordinate system. The

stagnation point was located on each photograph as indicated in figure 5. The optical sighting device was used to locate and record approximately 70 points along each shock. Step sizes between points were approximately 0.06 inch. The silhouette of the model symmetry plane was also digitized from the schlieren photograph and recorded in the same manner as the shock, and in the correct relation to the shock. The digitized data from each photograph were stored in an individual file on a 5-1/4 inch floppy disk and later plotted by a graphics plotter. An indication of the accuracy of the process can be seen in figure 6 where at the smallest stand-off distance (near the stagnation point), repeatability is within approximately 5 percent and is better at larger stand-off distances.

RESULTS AND DISCUSSIONS

The shock shape and stand-off distance in Mach 6 air as a function of angle of attack (α) for two Reynolds numbers are shown in figures 7 and 8. (Notice that α is referenced to the Z axis, fig. 1.) Variations in a given shock were always smooth and minor inflections such as can be seen near the stagnation point in figure 7(c) are artifacts of the digitizing process. The stand-off distance is greatest at $\alpha = 10°$ (over most of the body) and decreases as α decreases to -10°. This is expected because $\alpha = 10°$ presents a very blunt cross section to the oncoming flow whereas at $\alpha = -10°$, the configuration tends toward a slender body with respect to the flow. The variation in stand-off distance with α is most significant around the upper shoulder region where the distance at $\alpha = 10°$ is approximately twice the distance at $\alpha = -10°$. Near the stagnation point ($X/L = 0$, $Y/L = 0$) the $\alpha = 10°$ distance exceeds the $\alpha = -10°$ distance by only about 30 per cent.

The HALIS computer code was utilized to compute the shock characteristics in $M = 6$ air for $\alpha = 0°$, $5°$, and $-5°$. The input flow conditions for HALIS were nominal wind tunnel values of M_∞ and γ_∞, since the air behaved ideally. Nominal values of M_∞ in Tables I(a) and (b) varied by less than 0.7 percent from run to run. Comparisons with the measured shocks are presented in figure 9. The computed shapes are in good agreement with the measurements except for a slight divergence in the lower shoulder region located about one-third body diameter away from the surface. The computed stand-off distances agree within about 5 per cent with measurements over the front surface except at the upper ellipsoidal section for $\alpha = 5°$ where agreement is within about 10 percent. The measured shocks in figure 9 are for $N_{Re,\infty} = 2 \times 10^6$/ft, and the calculations are independent of $N_{Re,\infty}$ since HALIS is an inviscid flow code. Within the range investigated in this study, $N_{Re,\infty}$ does not have an effect on the measured shock characteristics as illustrated in figure 10.

The variation in measured shock shapes and stand-off distances with angle of attack in $M = 6$ air is summarized in figure 11. It is clear from this comparison that decreasing α from 10° to -10° results in a smaller stand-off distance over most of the forebody.

Measured shock shapes in $M = 6$ CF_4 are shown in figure 12 for $N_{Re,\infty} = 0.5 \times 10^6$/ft, and in figure 13 for $N_{Re,\infty} = 0.3 \times 10^6$/ft. By comparing these results with those in figure 8, the shocks in the CF_4 flow are observed to be much closer to the body than for the corresponding angles of attack in air. The agreement between the measured data and the predictions from the HALIS code is good over the face of the model as illustrated for two angles of attack in figure 14. Disagreement is significant, however, away from the

shoulder. As in air, the effect of $N_{Re,\infty}$ over the small range obtainable in the CF_4 tunnel is shown to be negligible for $\alpha = 0°$ in figure 15. This same result can be shown for all values of α by overlaying respective parts of figures 12 and 13. Figure 16 presents a summary of angle-of-attack effects on the measured shock shapes in CF_4. For $-10° < \alpha < 10°$, the shocks appear to merge near the tangency point of the ellipsoid and the conical section. As previously mentioned, one of the most obvious differences between the air and CF_4 data is the shock stand-off distance. This difference is illustrated in figure 17 for $\alpha = 0°$, $10°$, and $-10°$. This effect, due to differences in density ratio across the shock, results in a shock stand-off distance in CF_4 that is less than half the distance in air. A slight inward deflection in the CF_4 shock can be detected in the region where the flow expands off the ellipsoid section into the conical section. This effect was observed as a decrease in local pressure in measured pressure distributions by Micol in reference 11.

In the two $M_\infty = 6$ wind tunnels used in this study, the normal shock density ratios were approximately 5 and 12 for air and CF_4, respectively. In the actual flight case (near perigee) where dissociation greatly reduces the post shock temperature, the density ratio is expected to be approximately 17. The HALIS code, with the assumption of thermochemical equilibrium, was used to compute the shock shape for $M_\infty = 31$ flight. This result is compared with the wind-tunnel air and CF_4 data (from fig. 17) in figure 18. The predicted shock stand-off distance in flight is even less than the measured CF_4 results as expected. Viscous and nonequilibrium flow effects as discussed in reference 12 and expected in the AFE flight are not addressed by the HALIS code. The flight shock stand-off distance will influence radiant heating by

determining the volume of radiators and their proximity to the surface. Furthermore, convective heating would also be expected to vary with stand-off distance due to stronger flow gradients, and the flow chemistry. Because the surface pressure distribution over the face of the vehicle will be influenced by the shock characteristics, the aerodynamics of the vehicle will be influenced as well.

CONCLUSIONS

Schlieren photographs were obtained for the AFE configuration in Mach 6 air and Mach 6 CF_4 for the angle-of-attack range $-10° < \alpha < 10°$. Shock shapes and stand-off distances were obtained by digitizing and storing the photographic information in a computer and plotting the results on a graphics plotter. The inviscid-flow computer code HALIS was used to predict the shock characteristics, and comparisons were made with the measured values for selected conditions. For the environments and range of conditions of the present study, the following conclusions are made:

1. Increasing the density ratio across the normal shock from approximately 5 (air) to approximately 12 (CF_4) resulted in a decrease in shock stand-off distance over the entire forebody being approximately 60 per cent in the stagnation region.
2. In CF_4 a slight inward deflection of the shock occurs near the forebody ellipsoid/cone junction indicating a greater flow expansion in CF_4 ($\gamma_2 \approx 1.1$) than in air ($\gamma_2 = 1.4$).
3. As the angle of attack is decreased, the shock lies progressively closer to most of the forebody in both air and CF_4.

4. Variation in free-stream Reynolds number did not affect the shock at any angle of attack in air or CF_4 for the small range of this study.

5. Predictions from the inviscid-flow computer code HALIS were in good agreement with the measured values over the face of the model in both air and CF_4.

REFERENCES

1. Walberg, G. D.: A Review of Aeroassisted Orbit Transfer, AIAA Paper 82-1378, AIAA 9th Atmospheric Flight Mechanics Conference, San Diego, California, August 9-11, 1982.

2. Jones, J. J.: The Rationale for an Aeroassist Flight Experiment. AIAA Paper No. 87-11508, June 8, 1987.

3. Wells, W. L.: Wind Tunnel Preflight Test Program for Aeroassist Flight Experiment. AIAA Paper No. 87-2367-CP, August 1987.

4. Walberg, G. D., Siemers, P. M., III, Calloway, R. L., and Jones, J. J.: The Aeroassist Flight Experiment. Paper presented at the 38th International Astronautical Federation Congress, Brighton, England, Paper No. IAF 87-197, October 10-17, 1987.

5. Gamble, J., Cerimele, C., and Spratlin, K.: Aerobraking of a Low L/D Manned Vehicle from GEO Return to Rendezvous with the Space Shuttle, AIAA Paper 83-2110, AIAA Atmospheric Flight Mechanics Conference, Gatlinburg, Tennessee, August 15-17, 1983.

6. Cheatwood, F. M., DeJarnette, F. R., and Hamilton, H. H., II: Geometrical Description for a Proposed Aeroassist Flight Experiment Vehicle, NASA TM 87714, July 1986.

7. Miller, C. G., III and Gnoffo, P. A.: Pressure Distributions and Shock Shapes for 12.84°/7° On-Axis and Bent-Nose Biconics in Air at Mach 6. NASA TM 83222, December 1981.

8. Midden, R. E., and Miller, C. G. III: Description and Calibration of the Langley Hypersonic CF_4 Tunnel. NASA TP-2384, March 1985.

9. Weilmuenster, J. K., and Hamilton, H. H., III: A Comparison of Computed and Measured Aerodynamic Characteristics of a Proposed Aeroassist Experiment Configuration. NASA TM 89034, January 1987.

10. Sutton, Kenneth: Relations for the Thermodynamic and Transport Properties in the Testing Environment of the Langley Hypersonic CF_4 Tunnel, NASA TM 83220, October 1981.

11. Micol, J. R.: Simulation of Real Gas Effects on Pressure Distributions for a Proposed Aeroassist Flight Experiment Vehicle and Comparison to Prediction. AIAA Paper 87-2368, AIAA Atmospheric Flight Mechanics Conference, Monterey, California. August 17-19, 1987.

12. Miller, C. G., Micol, J. R., and Gnoffo, P. A.: Laminar Heat-Transfer Distributions on Biconics at Incidence in Hypersonic-Hypervelocity Flows. NASA TP 2213, January 1985.

TABLE I. NOMINAL FREE-STREAM AND POSTNORMAL SHOCK FLOW CONDITIONS FOR THE LANGLEY 20-INCH MACH 6 TUNNEL.

(a) $N_{Re,1}$ = 0.6E+06/ft

Reservoir Stagnation Conditions

$p_{t,1}$	$T_{t,1}$	$\rho_{t,1}$
33.0	886.7	0.100

Free-Stream Conditions

p_1	T_1	ρ_1	M_1	$N_{Re,1}$	q_1
0.0245	113.2	5.86E-04	5.844	6.36E+05	0.587

Static Postnormal Shock Conditions

p_2	T_2	ρ_2	M_2	$N_{Re,2}$	γ_2
0.9737	858.4	3.06E-03	0.406	1.03E+05	1.40

Stagnation Postnormal Shock Conditions

$p_{t,2}$	$T_{t,2}$	$\rho_{t,2}$
1.090	886.7	3.31E-03

TABLE I. CONCLUDED

(b) $N_{Re,1}$ = 2.0E+06/ft

Reservoir Stagnation Conditions

$p_{t,1}$	$T_{t,1}$	$\rho_{t,1}$
123.3	925.8	0.360

Free-Stream Conditions

p_1	T_1	ρ_1	M_1	$N_{Re,1}$	q_1
0.0819	114.4	1.93E-03	5.954	2.13E+06	2.032

Static Postnormal Shock Conditions

p_2	T_2	ρ_2	M_2	$N_{Re,2}$	γ_2
3.373	896.4	0.010	0.405	3.37E+05	1.40

Stagnation Postnormal Shock Conditions

$p_{t,2}$	$T_{t,2}$	$\rho_{t,2}$
3.775	925.8	0.011

TABLE II. NOMINAL FREE-STREAM AND POSTNORMAL SHOCK FLOW CONDITIONS FOR THE LANGLEY HYPERSONIC CF_4 TUNNEL.

(a) $N_{Re,1}$= 0.3E+06/ft

Reservoir Stagnation Conditions

$p_{t,1}$	$T_{t,1}$	$\rho_{t,1}$
969.0	1164	6.62E+00

Free-Stream Conditions

p_1	T_1	ρ_1	M_1	$N_{Re,1}$	q_1
0.0262	300.1	7.15E-04	6.243	2.98E+05	0.630

Static Postnormal Shock Conditions

p_2	T_2	ρ_2	M_2	$N_{Re,2}$	γ_2
1.178	1151	8.40E-03	0.287	9.70E+04	1.11

Stagnation Postnormal Shock Conditions

$p_{t,2}$	$T_{t,2}$	$\rho_{t,2}$
1.233	1156	8.75E-03

TABLE II. CONCLUDED

(b) $N_{Re,1}$ = 0.5E+06/ft

Reservoir Stagnation Conditions

$p_{t,1}$	$T_{t,1}$	$\rho_{t,1}$
1496	1157	1.01E+01

Free-Stream Conditions

p_1	T_1	ρ_1	M_1	$N_{Re,1}$	q_1
0.0387	291.8	1.09E-03	6.294	4.63E+05	0.949

Static Postnormal Shock Conditions

p_2	T_2	ρ_2	M_2	$N_{Re,2}$	γ_2
1.774	1141	1.28E-02	0.287	1.48E+05	1.11

Stagnation Postnormal Shock Conditions

$p_{t,2}$	$T_{t,2}$	$\rho_{t,2}$
1.857	1146	1.33E-02

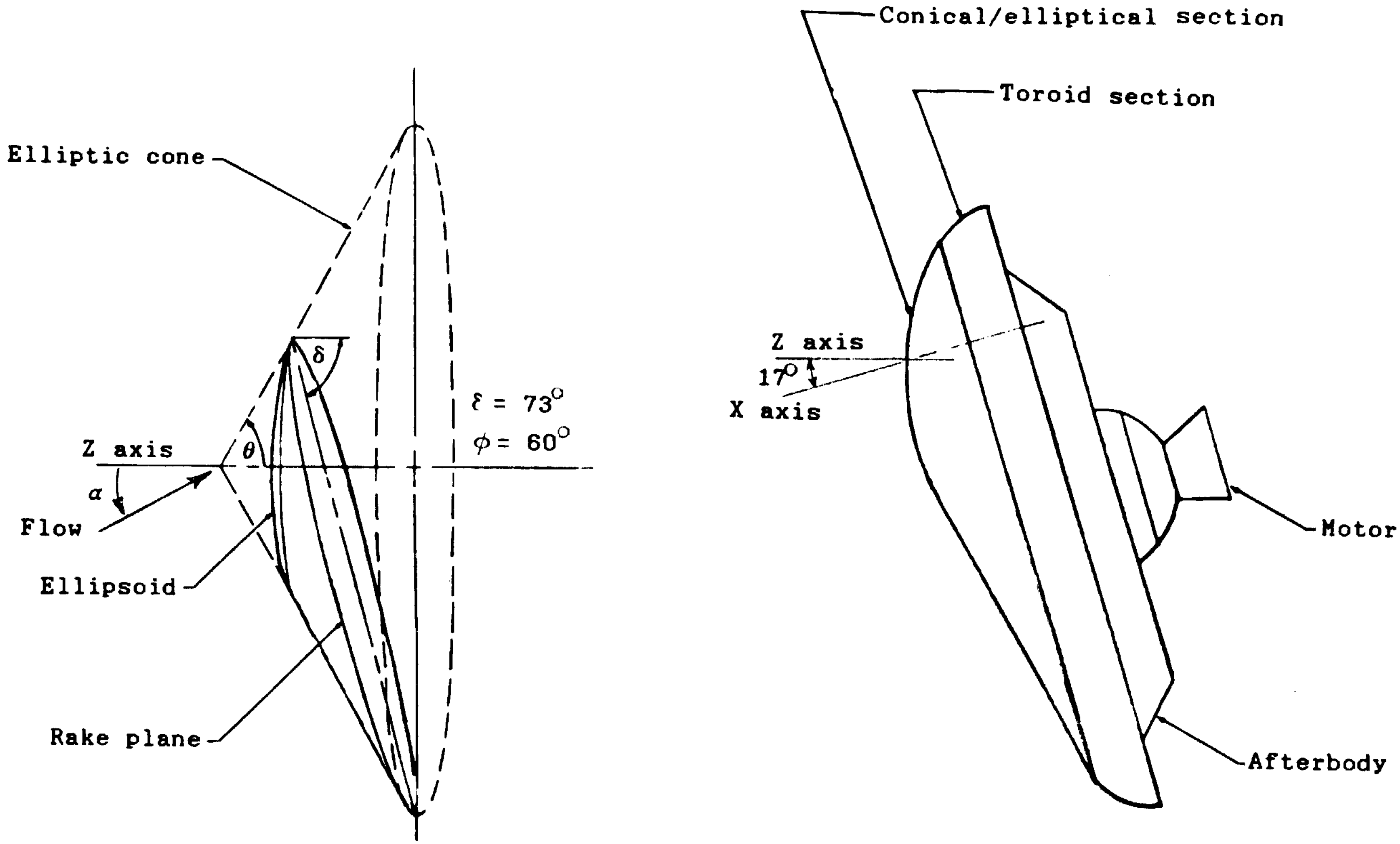

(a) Forebody development.

(b) Vehicle configuration.

Figure 1.- Development of AFE configuration from original elliptic cone.

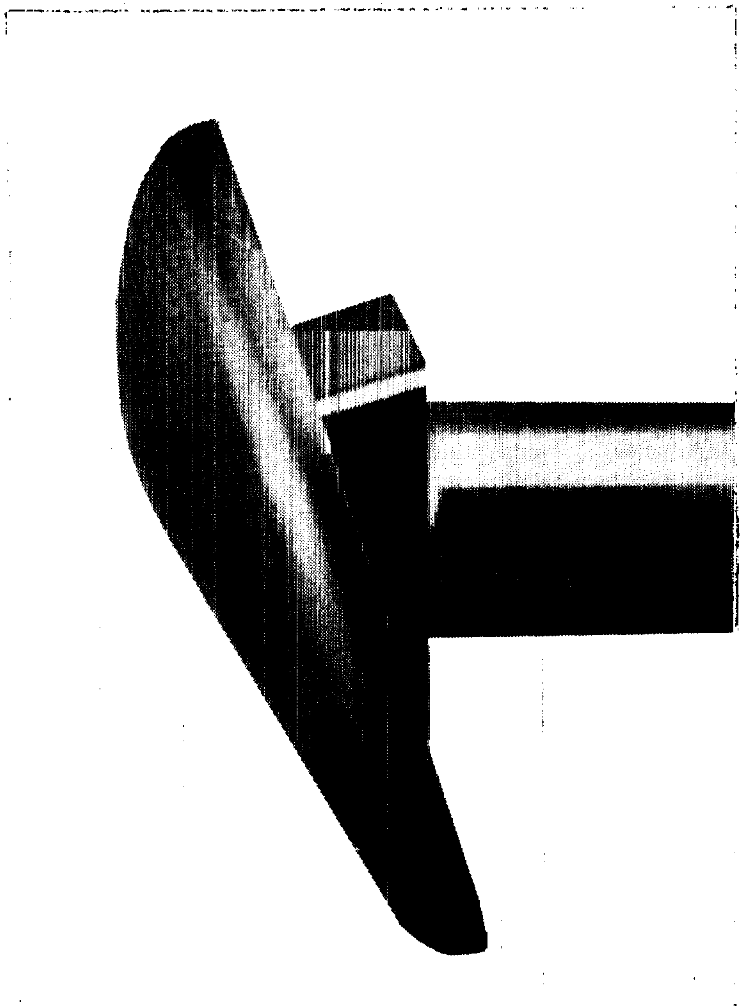

(a) Pressure model.

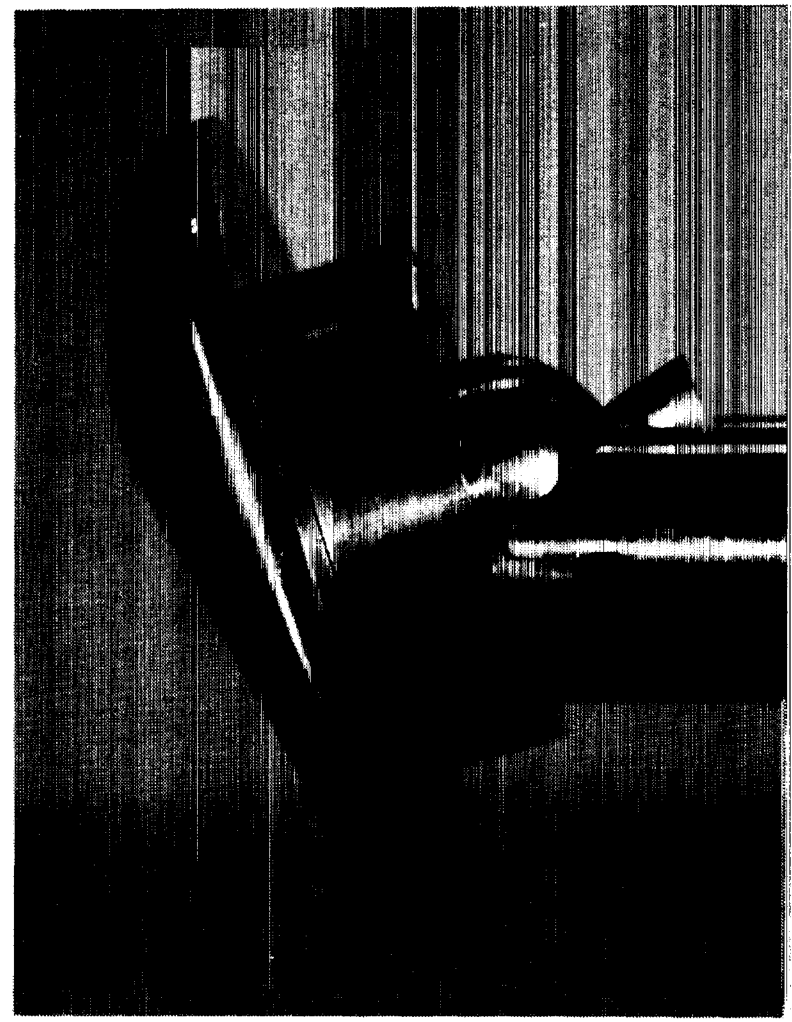

(b) Force and moment model.

Figure 2.- Photographs of wind-tunnel models used for schlieren photographs.

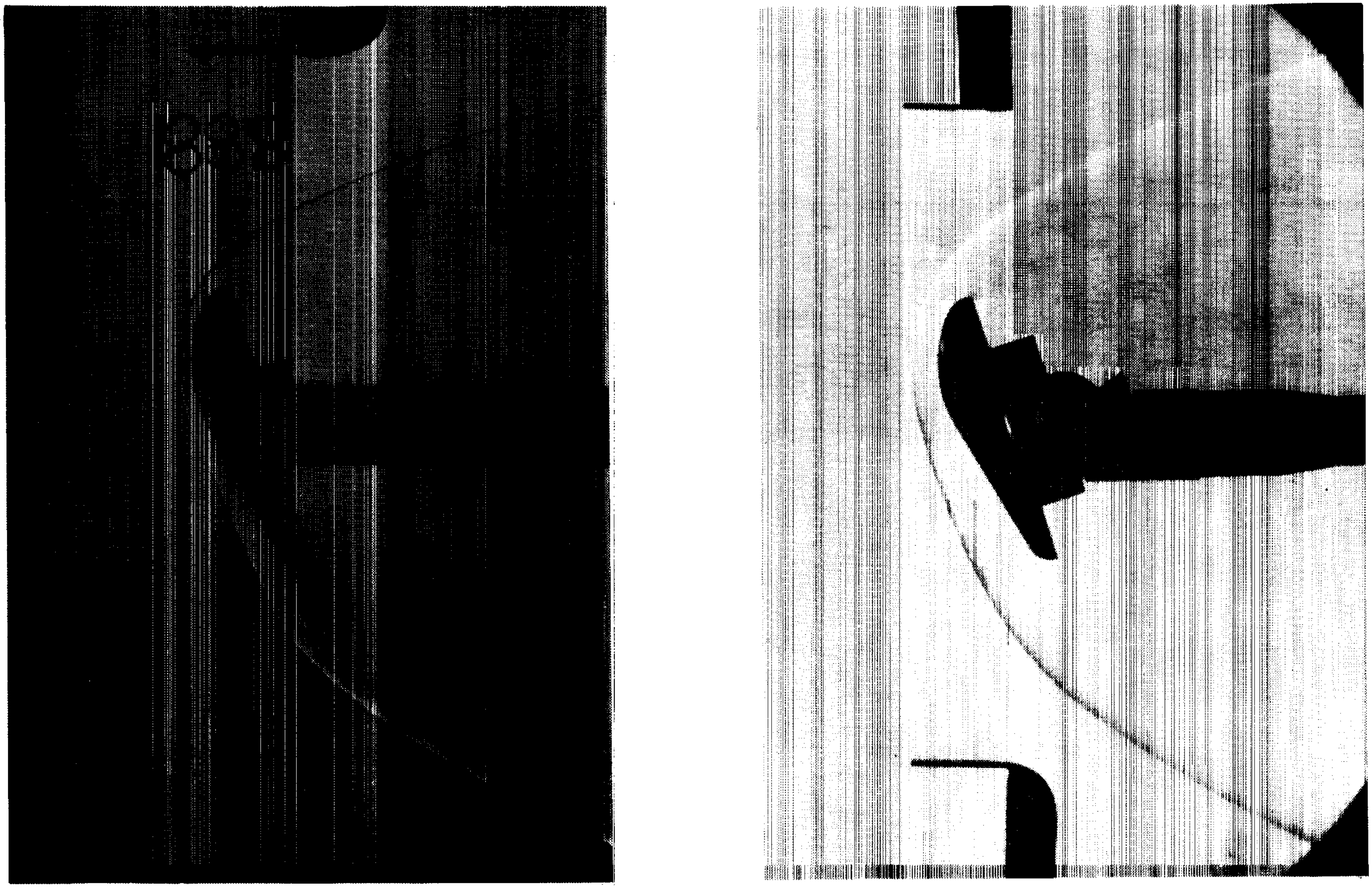

(a) Pressure model in CF_4.

(b) Force and moment model in air.

Figure 3.- Typical schlieren photographs for AFE at $M_\infty = 6$ and $\alpha = 0$.

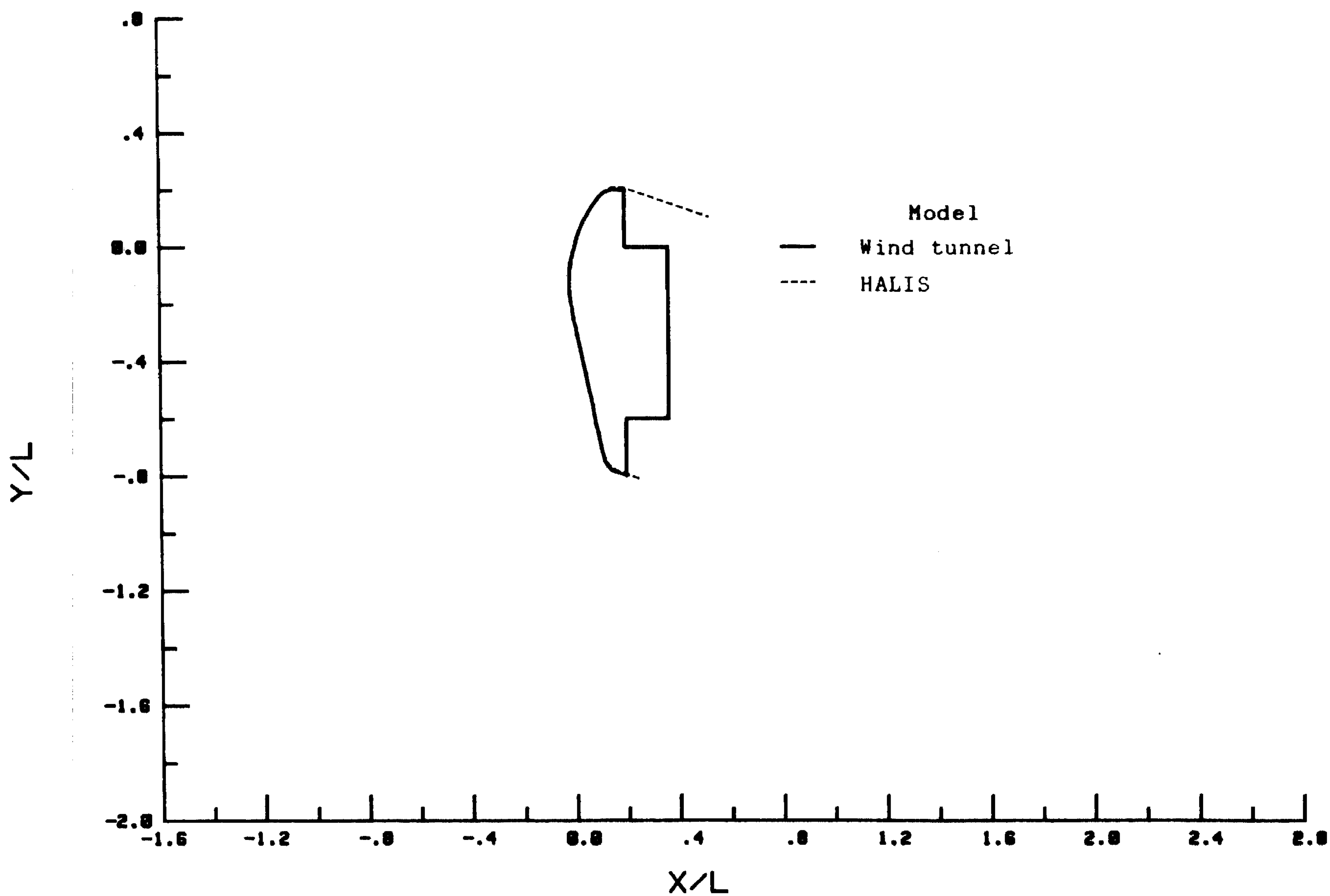

Figure 4.- Comparison of digitized shape of wind-tunnel model and numeric model.

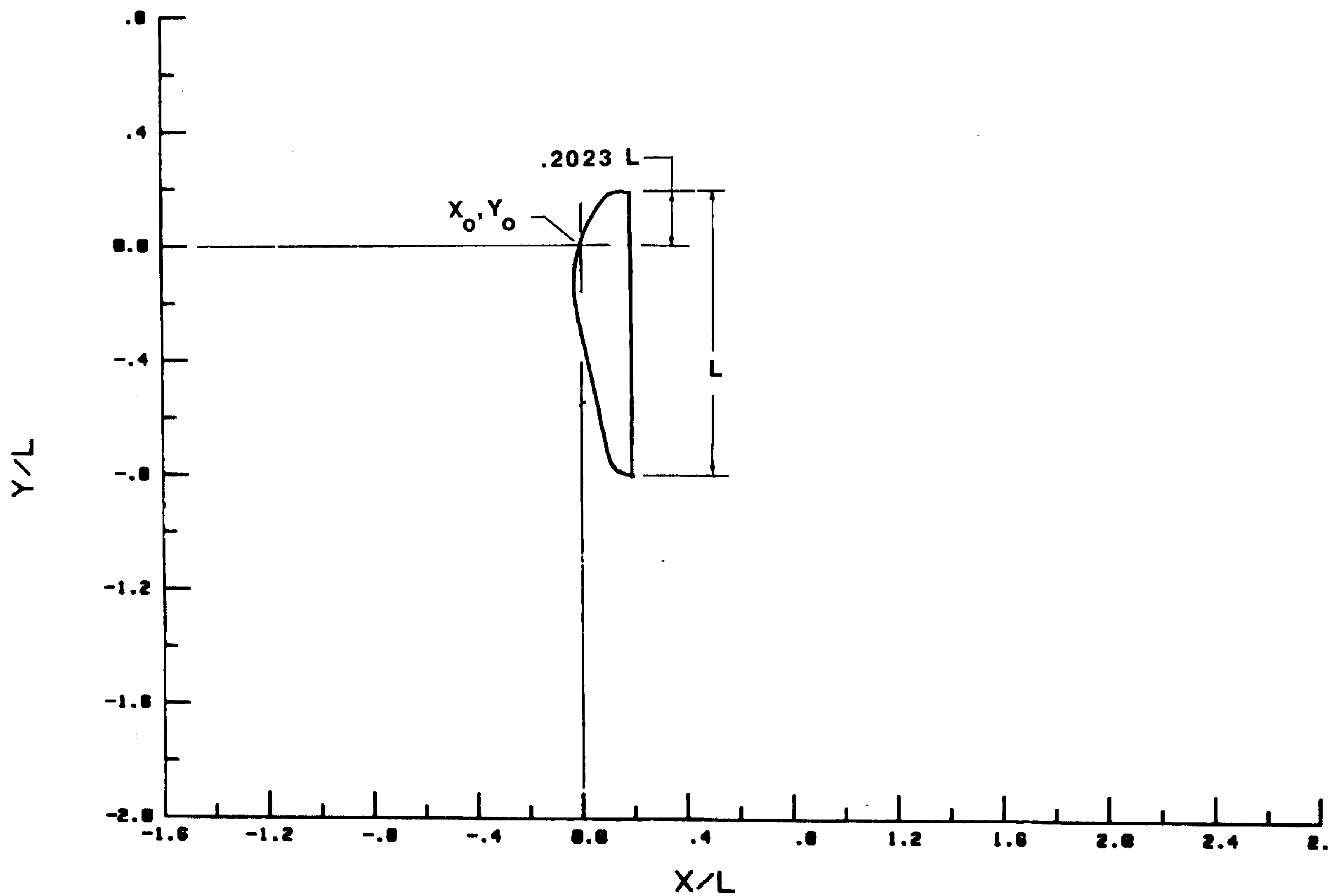

Figure 5.- Coordinate system for shock shape display.

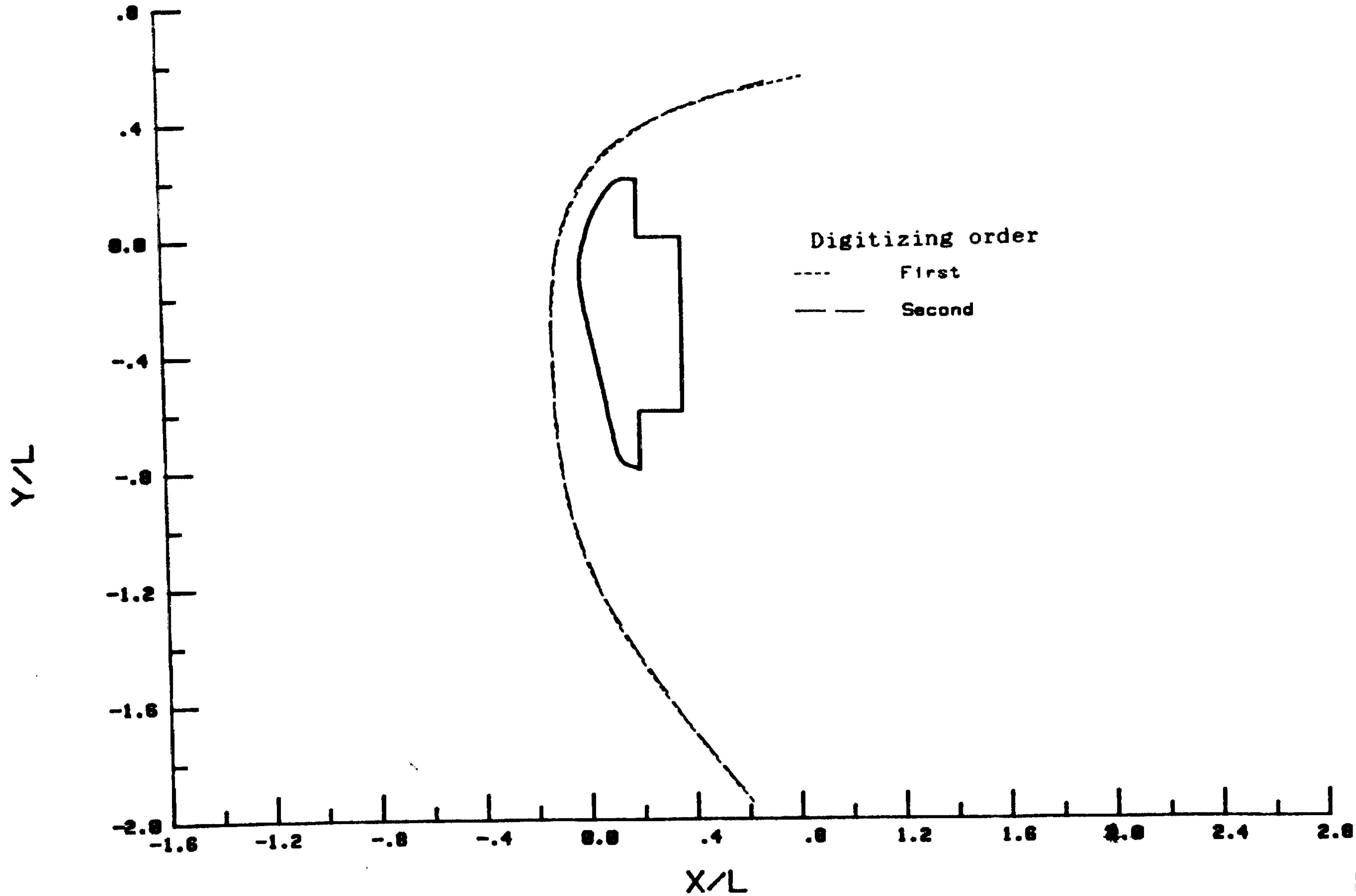

Figure 6.- Indication of accuracy due to digitizing process. LaRC 20-Inch Mach 6 Tunnel, $\alpha = 0°$, $N_{Re,\infty} = 0.6 \times 10^6$/ft in air.

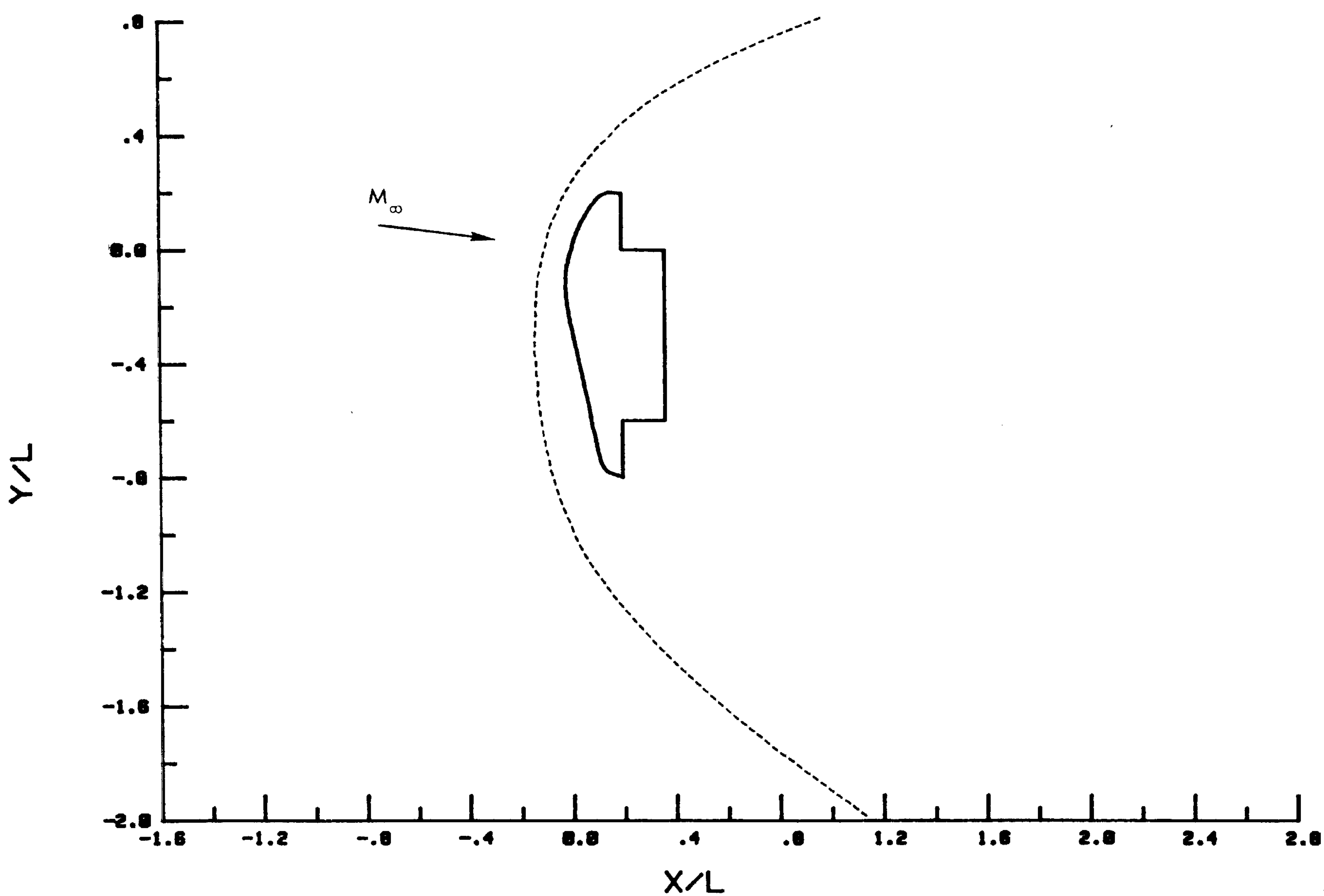

(a) α = 10°.

Figure 7.- Measured AFE shock shapes in M_∞ = 6 air at $N_{Re,\infty} = 2.0 \times 10^6$/ft.

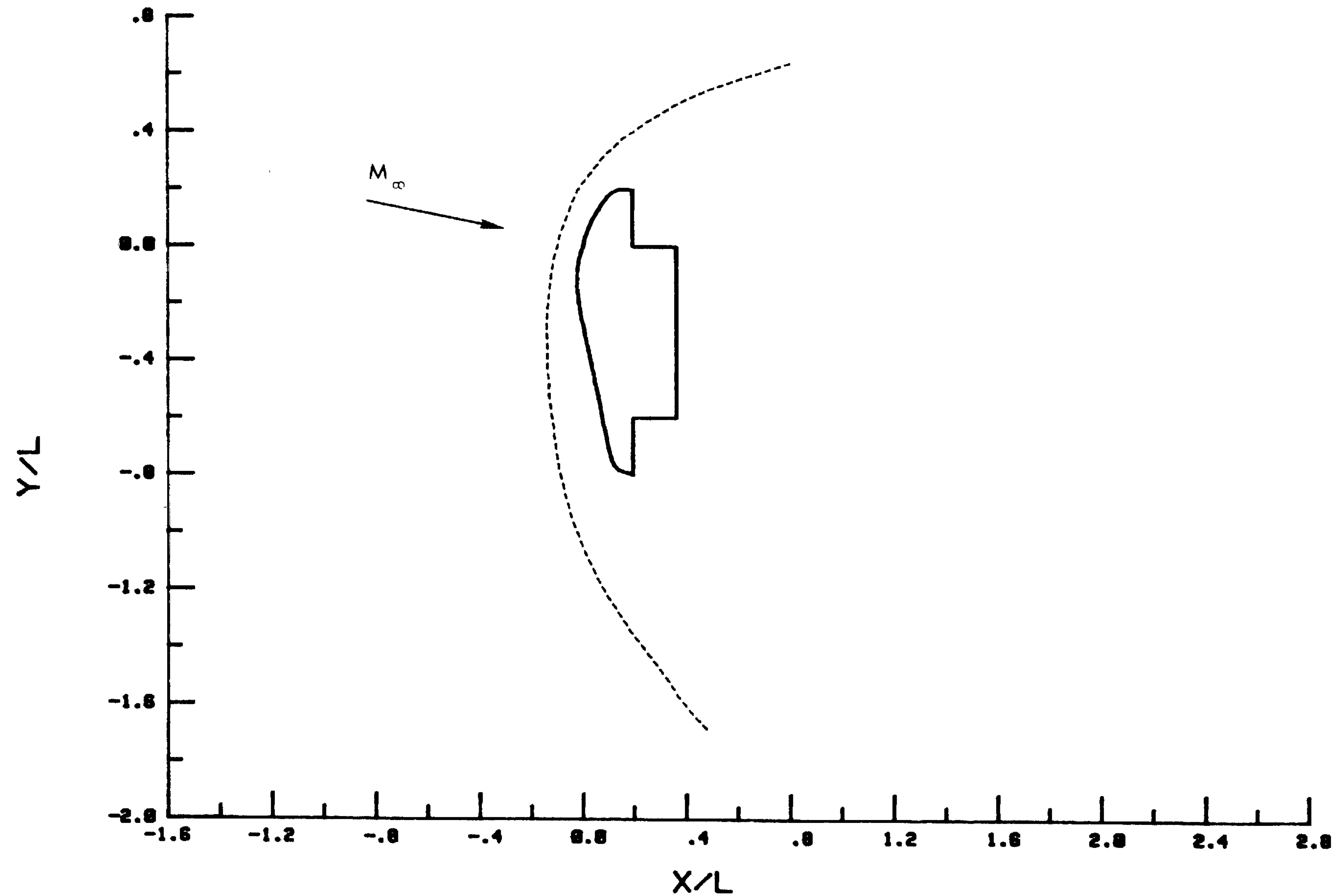

(b) $\alpha = 5°$.

Figure 7.- Continued.

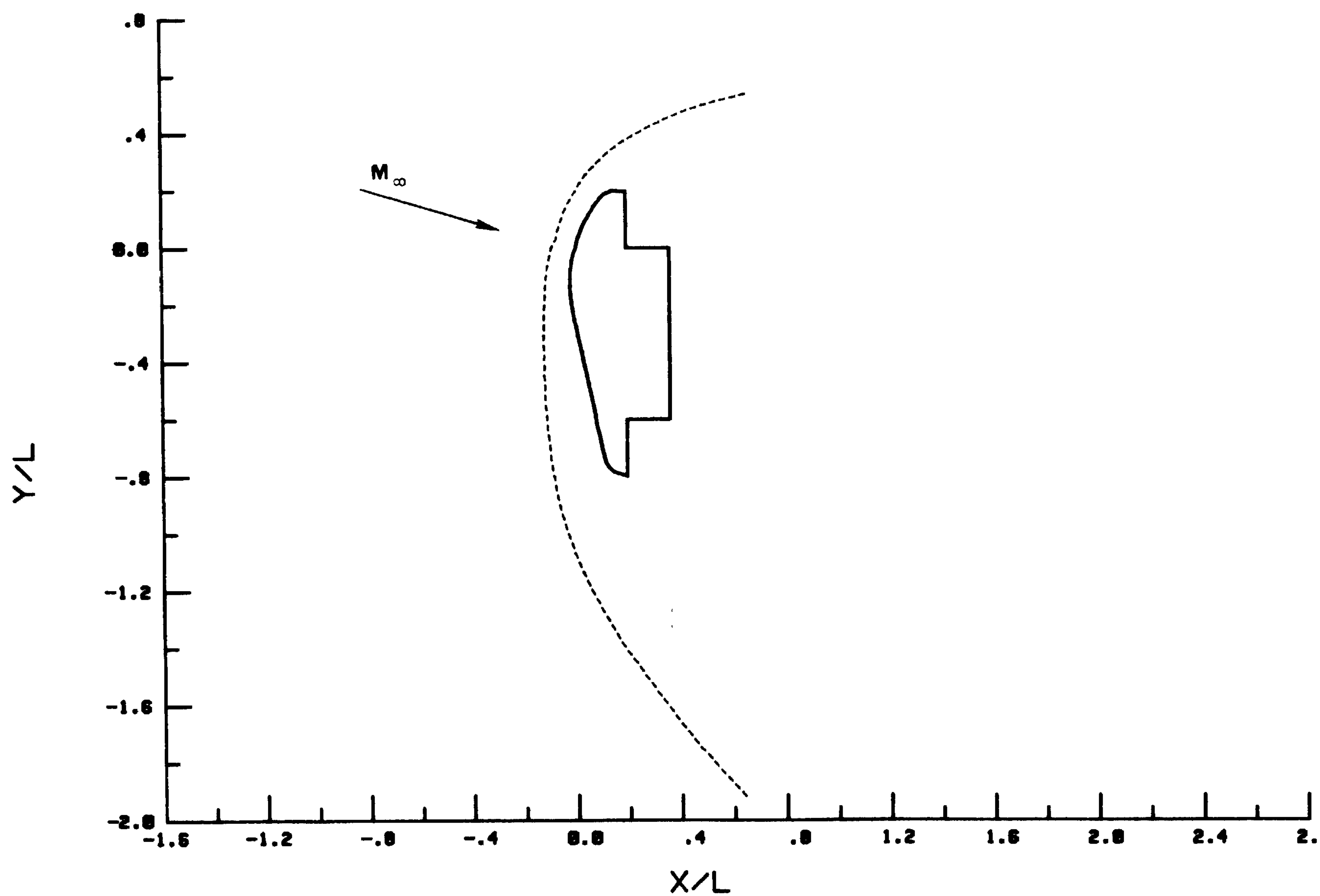

(c) α = 1° (α = 0° not available).

Figure 7.- Continued.

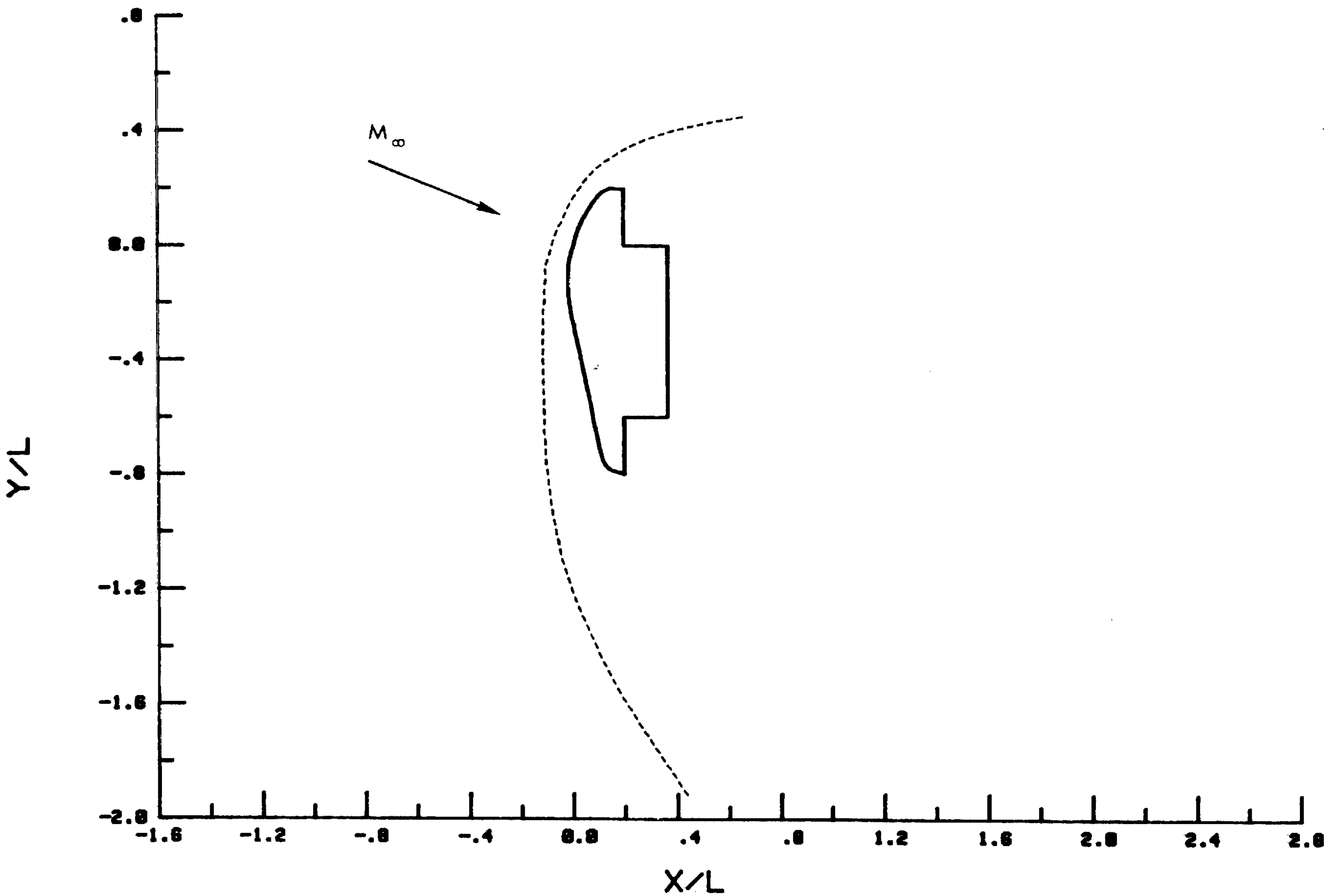

(d) $\alpha = -5°$.

Figure 7.- Continued.

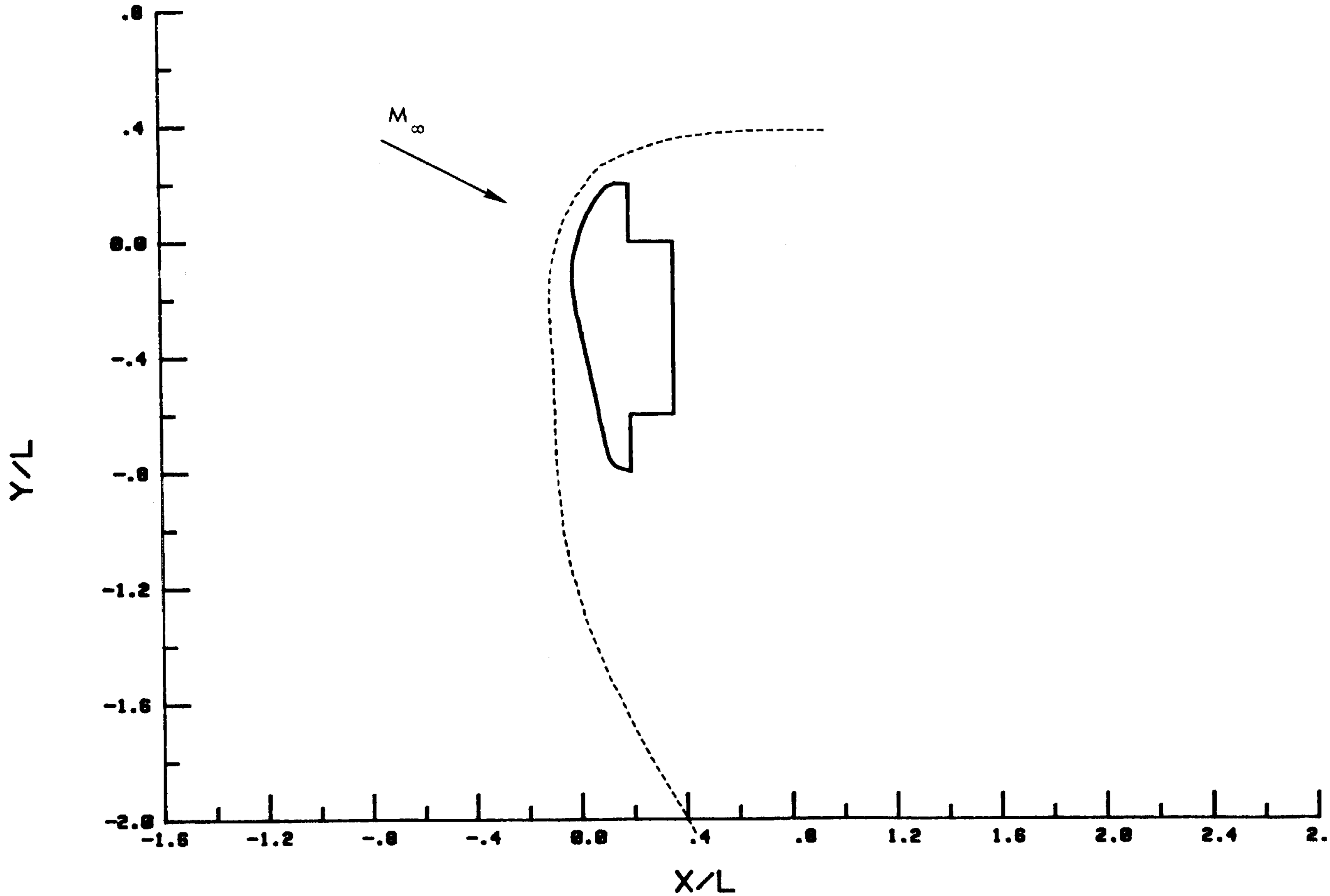

(e) $\alpha = -10°$.

Figure 7.- Concluded.

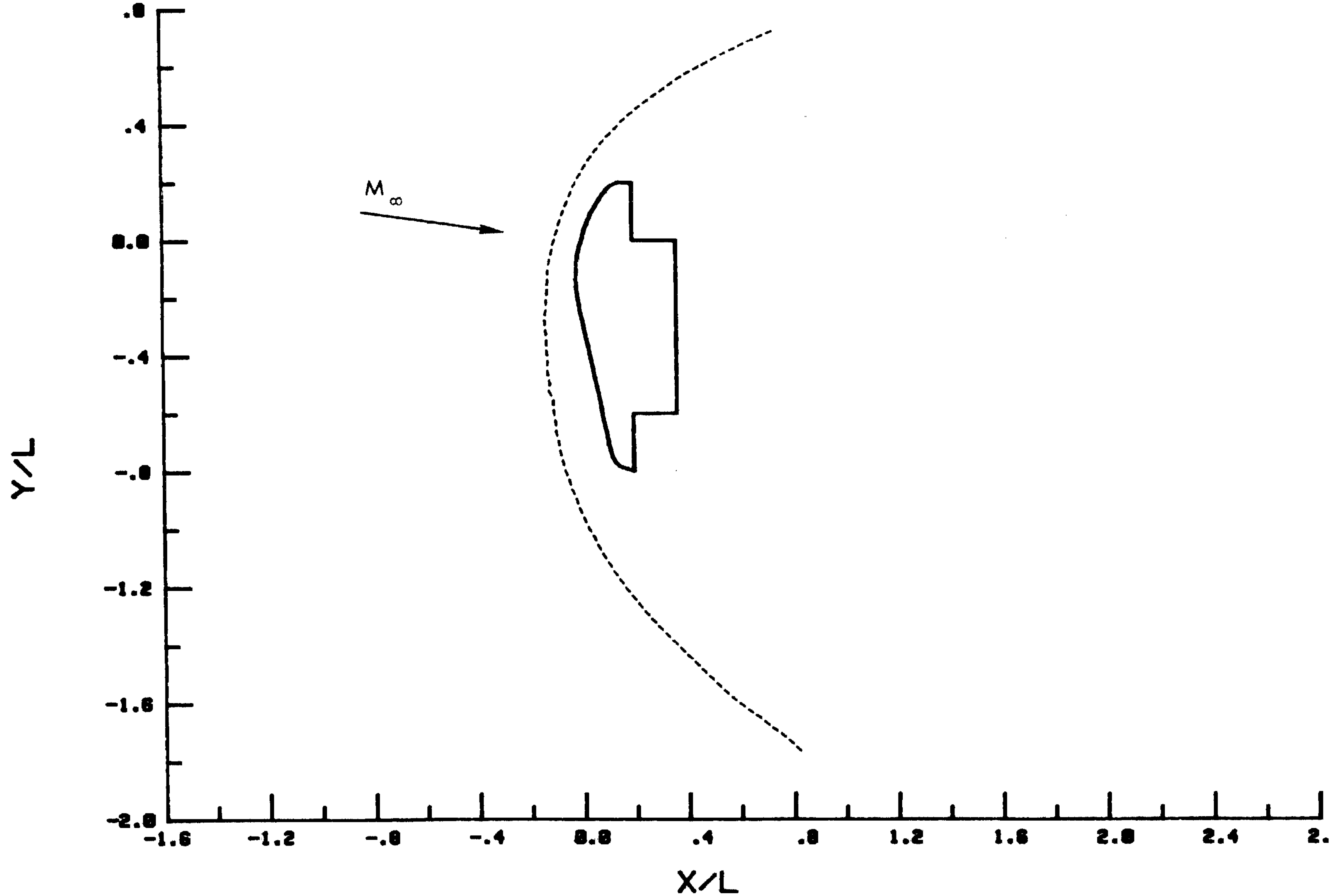

(a) $\alpha = 10°$.

Figure 8.- Measured AFE shock shapes in $M_\infty = 6$ air at $N_{Re,\infty} = 0.6 \times 10^6$/ft.

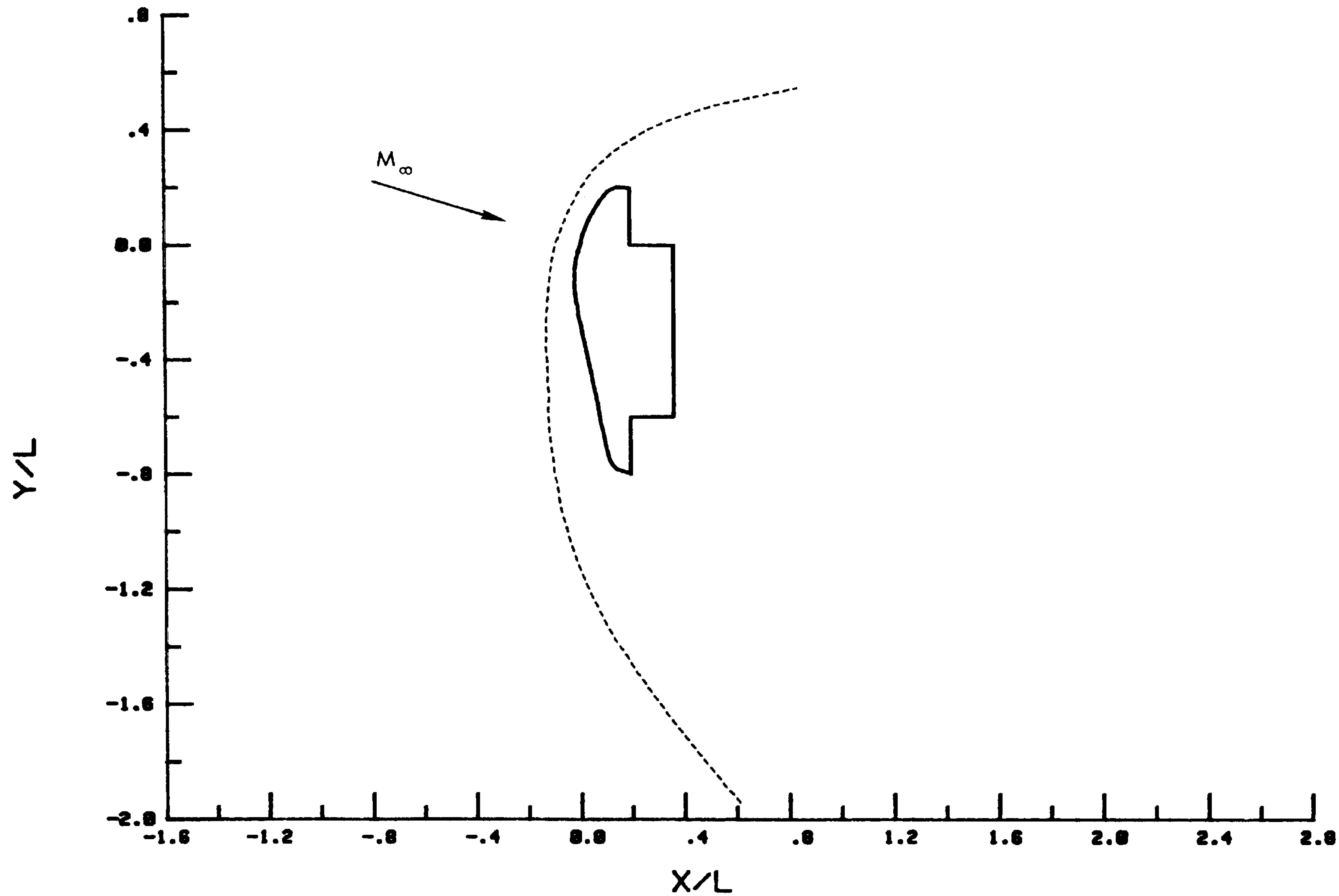

(b) $\alpha = 0°$.

Figure 8.- Continued.

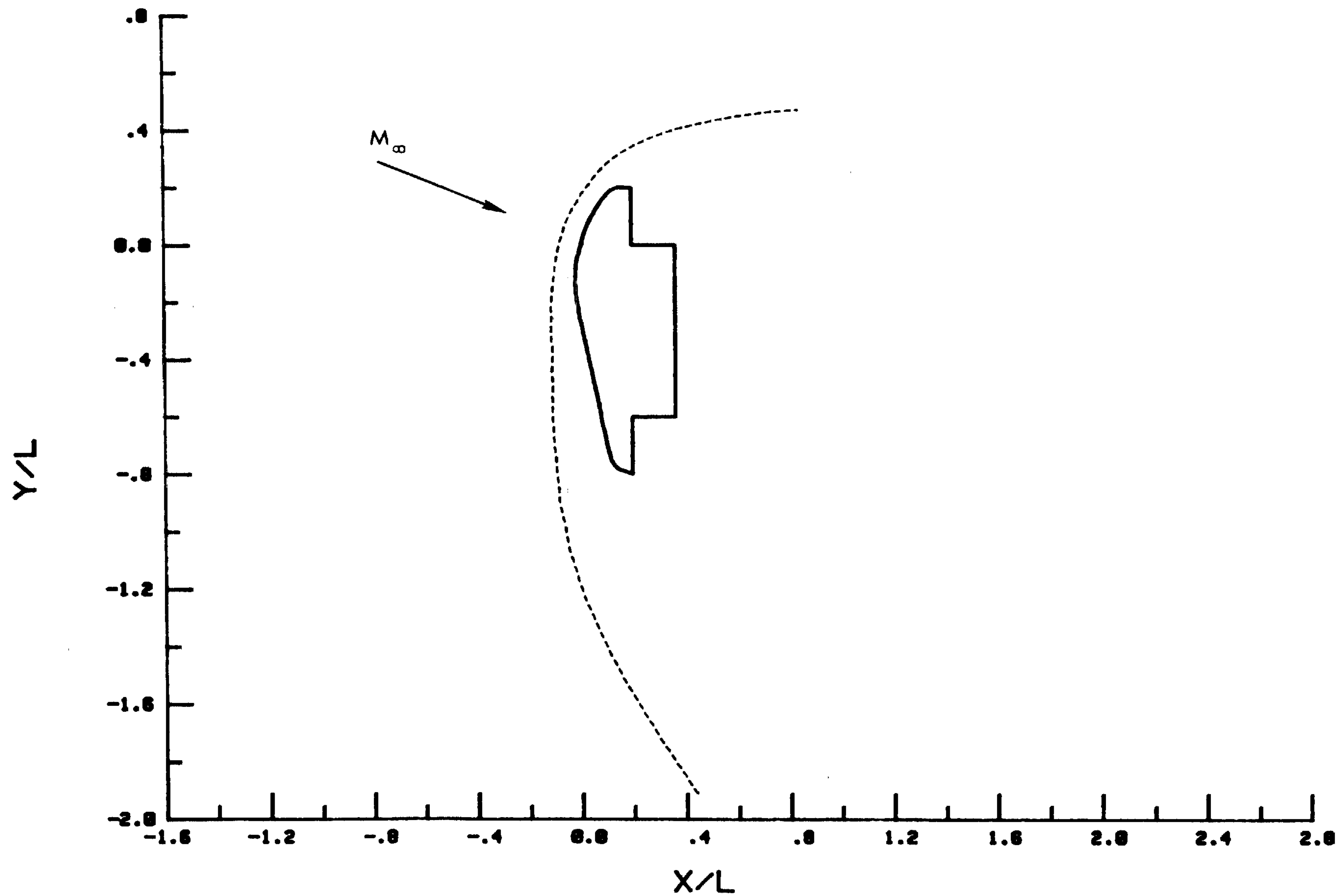

(c) $\alpha = -5°$.

Figure 8.- Continued.

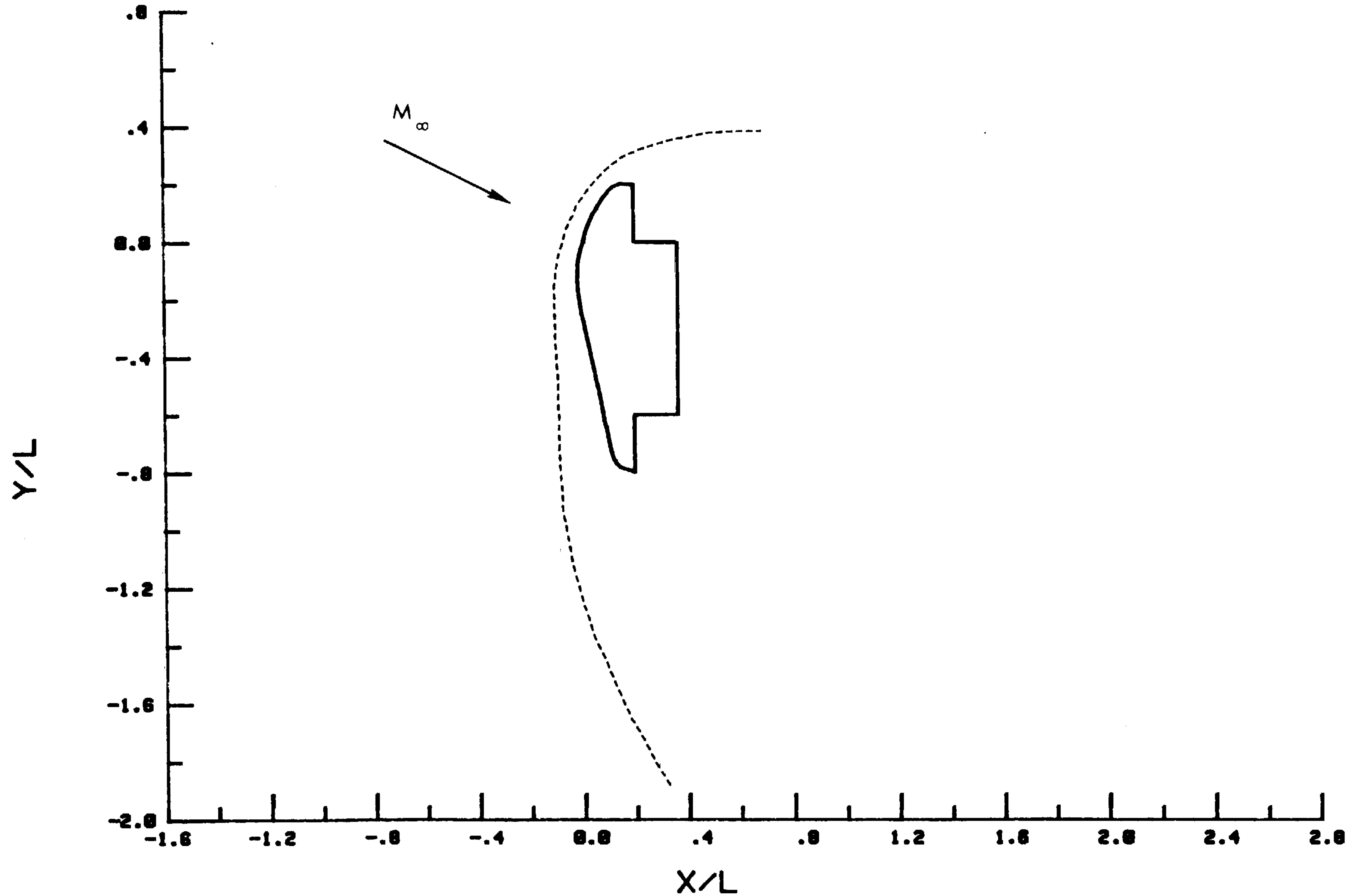

(d) $\alpha = -10°$.

Figure 8.- Concluded.

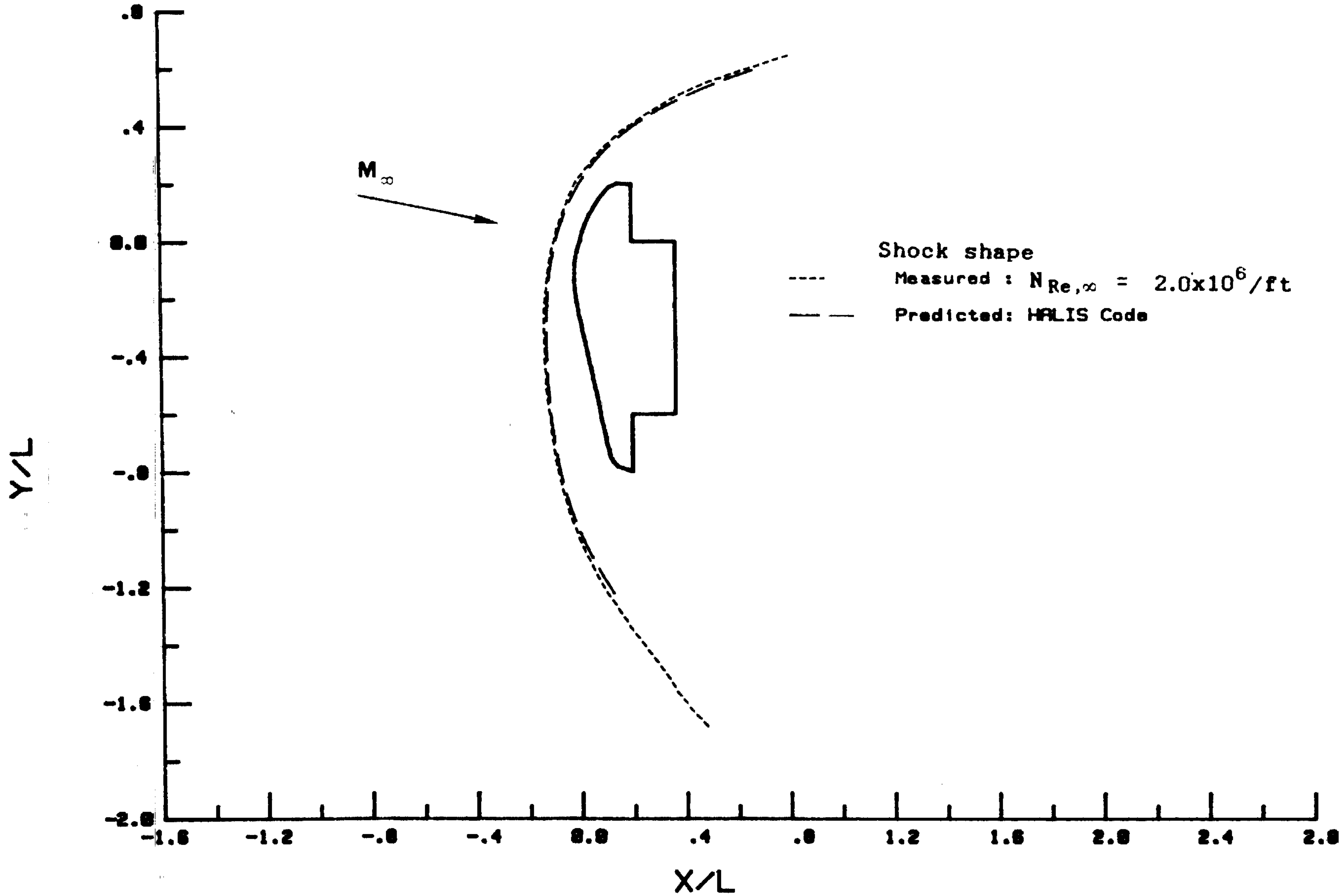

(a) $\alpha = 5°$.

Figure 9.- Comparison of predicted and measured shock shapes in $M_\infty = 6$ air.

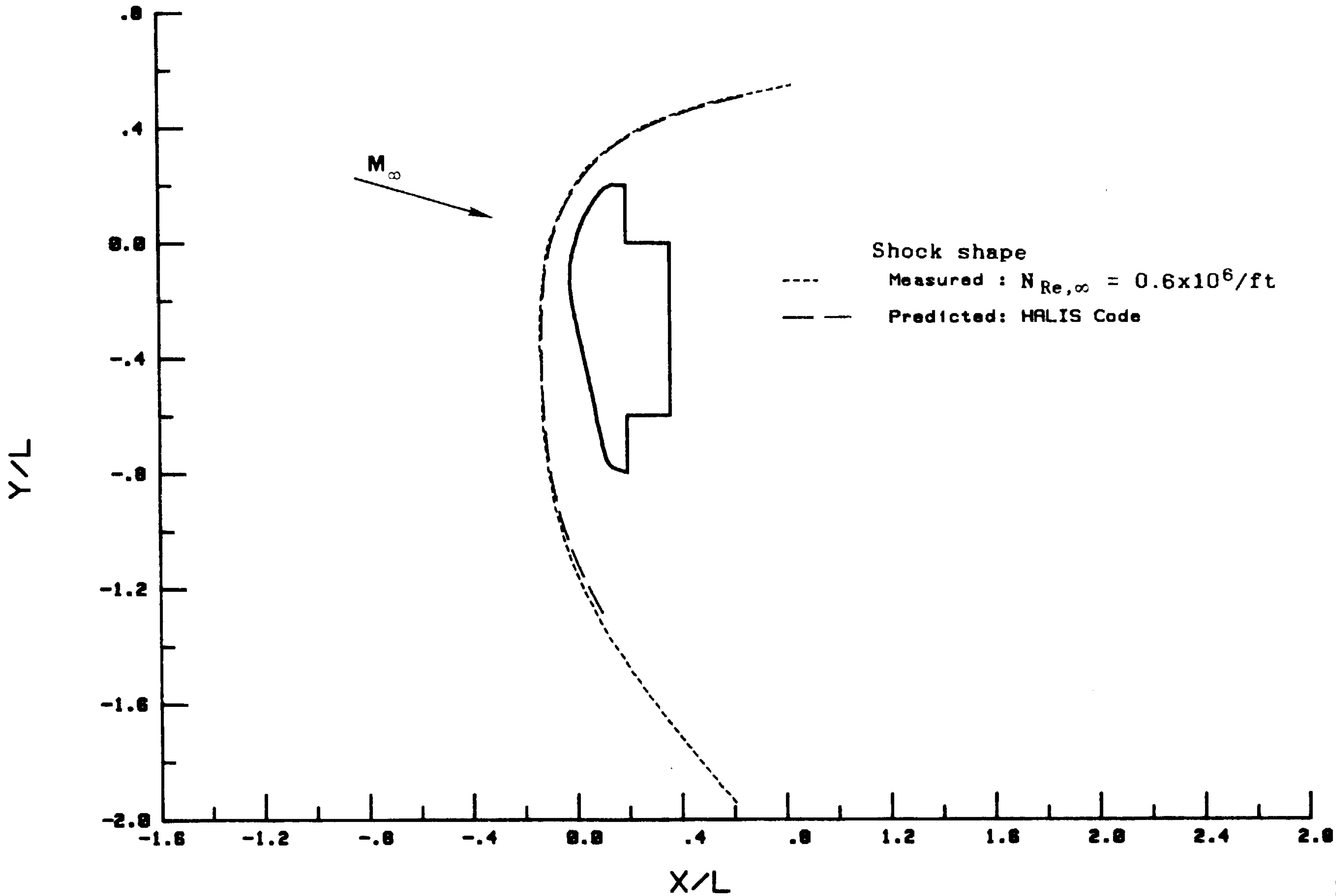

(b) α = 0°.

Figure 9.- Continued.

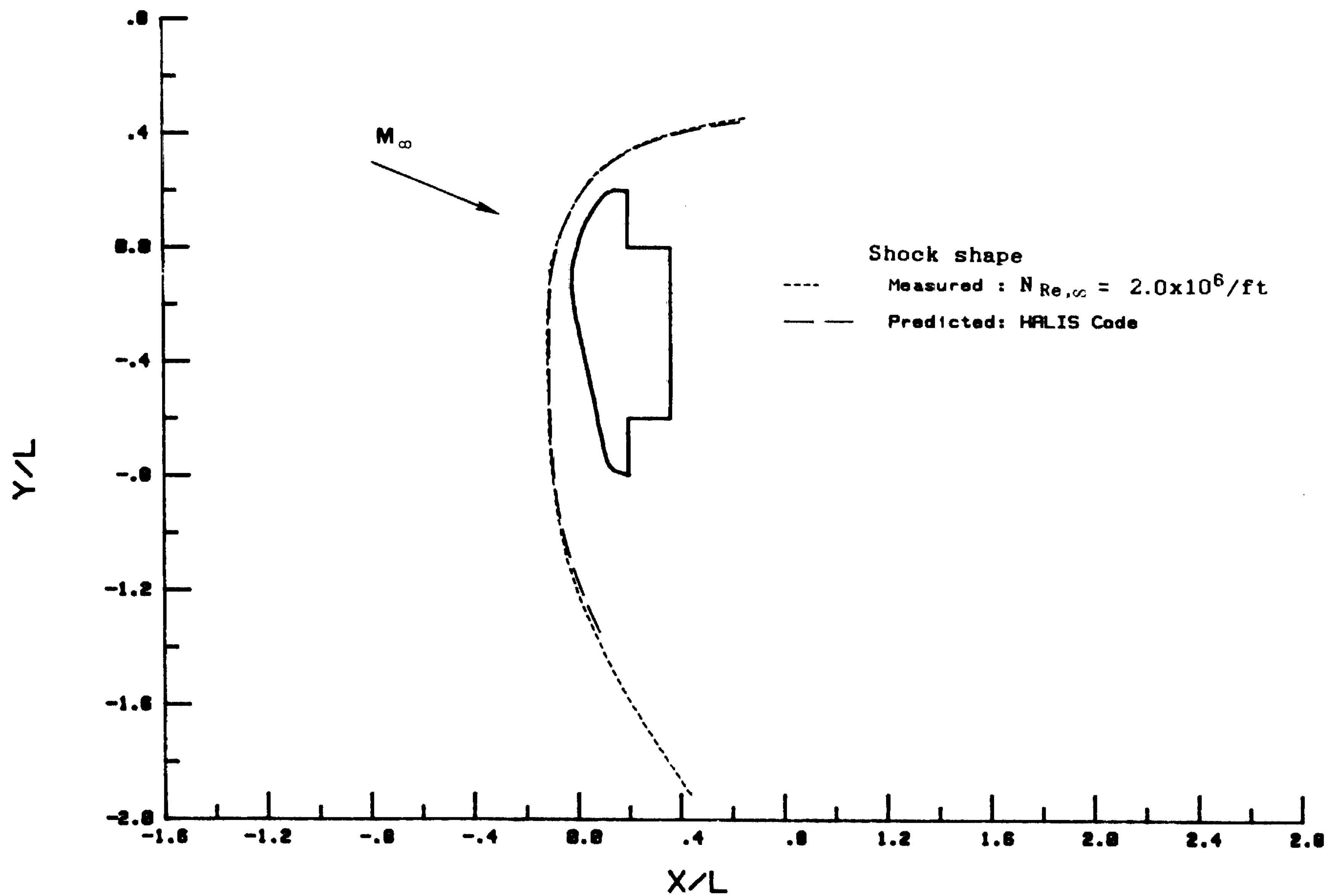

(c) $\alpha = -5°$.

Figure 9.- Concluded.

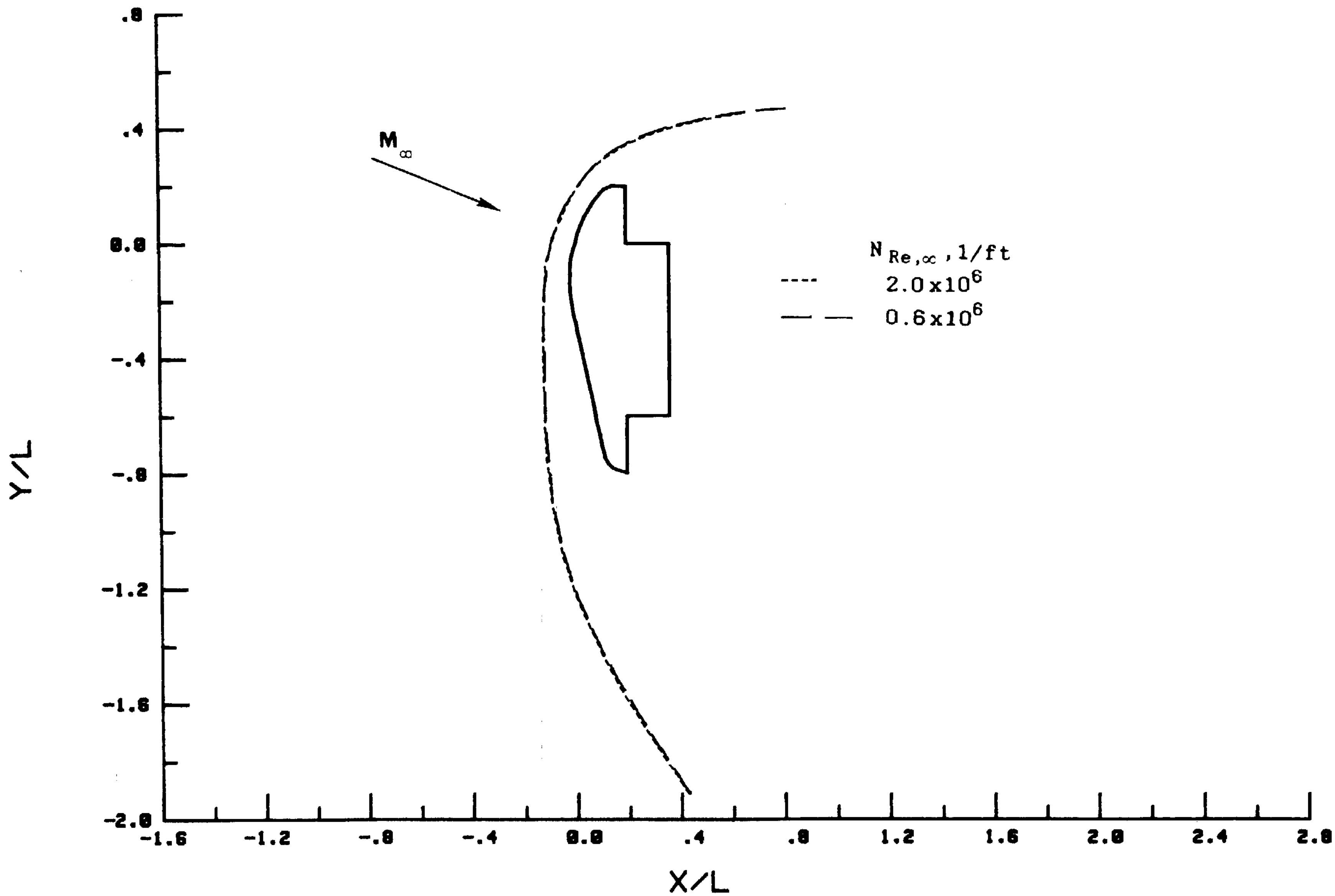

Figure 10.- Effect of $N_{Re,\infty}$ for $\alpha = -5°$ in $M_\infty = 6$ air.

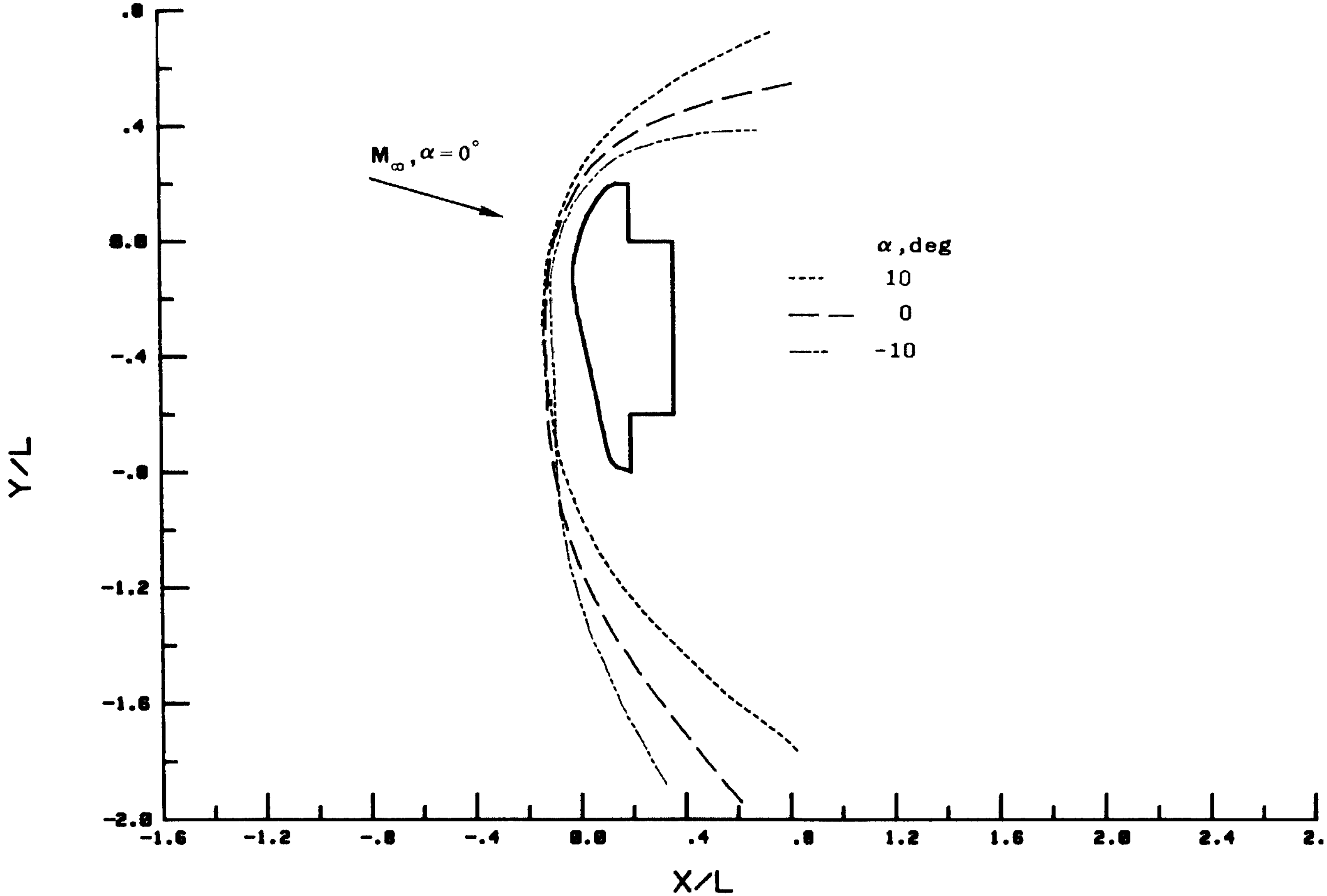

Figure 11.- Effect of α in $M_\infty = 6$ air.

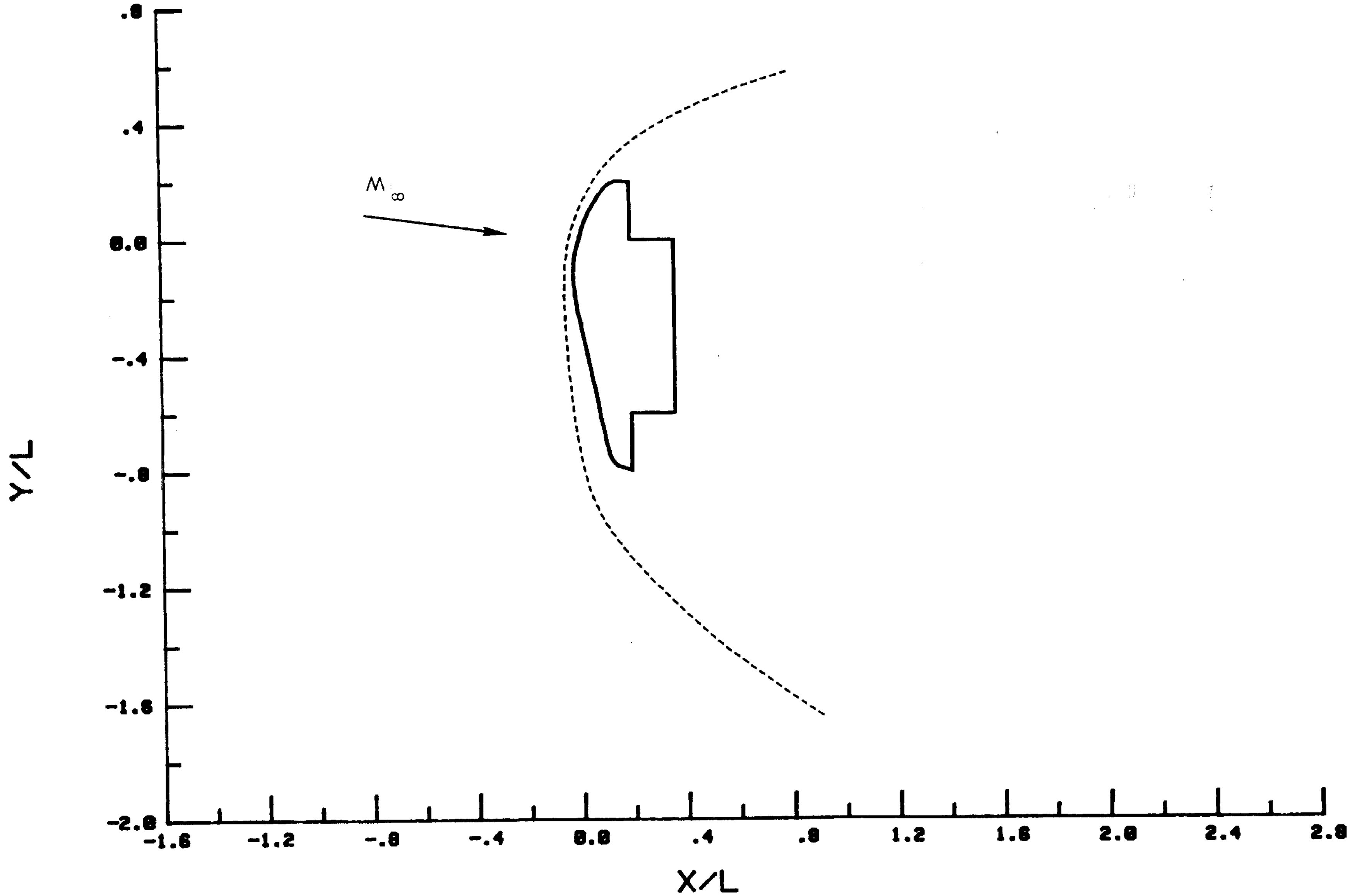

(a) $\alpha = 10°$.

Figure 12.- Measured AFE shock shape in $M_\infty = 6$ CF_4 at $N_{Re,\infty} = 0.50 \times 10^6$/ft.

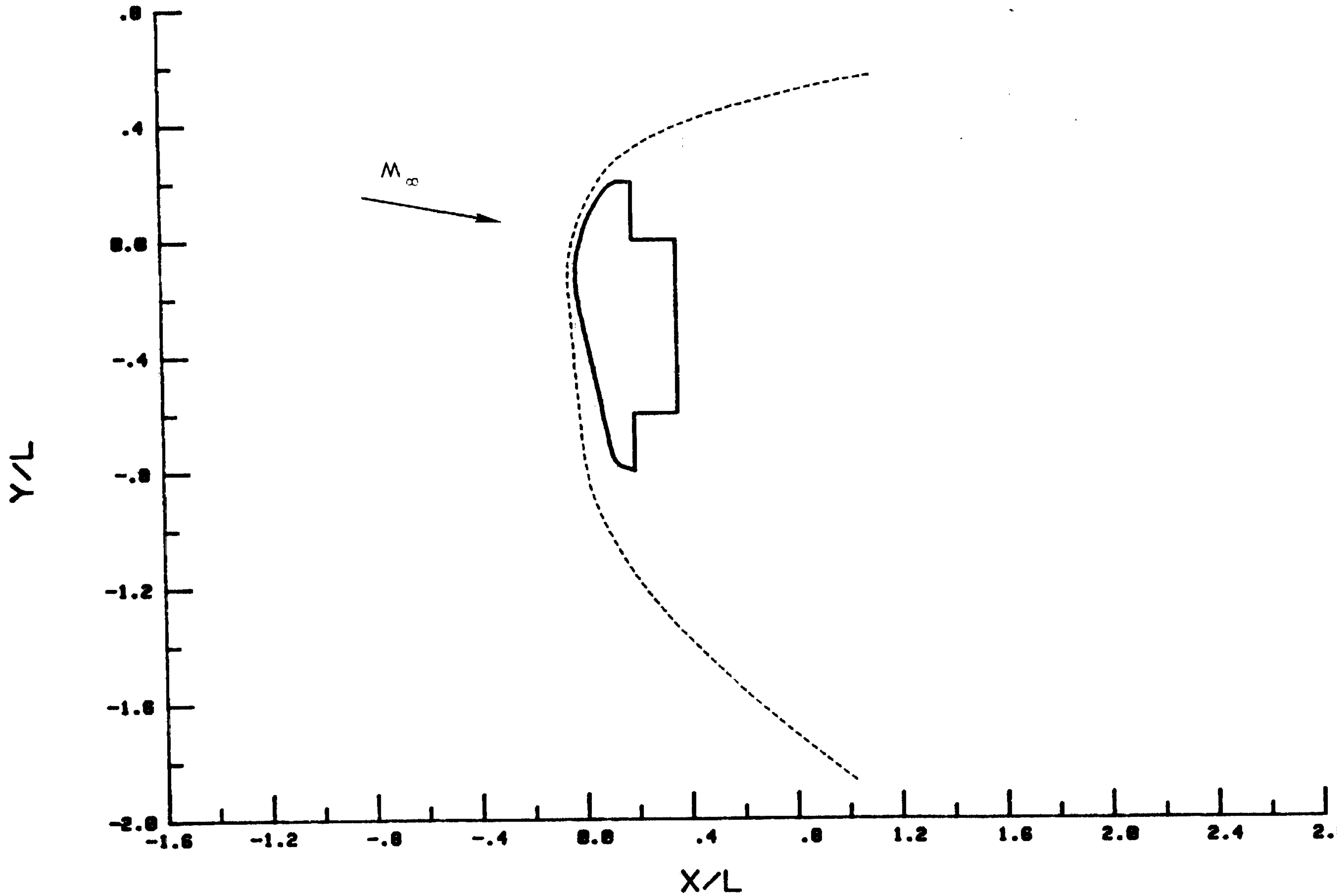

(b) $\alpha = 5°$.

Figure 12.- Continued.

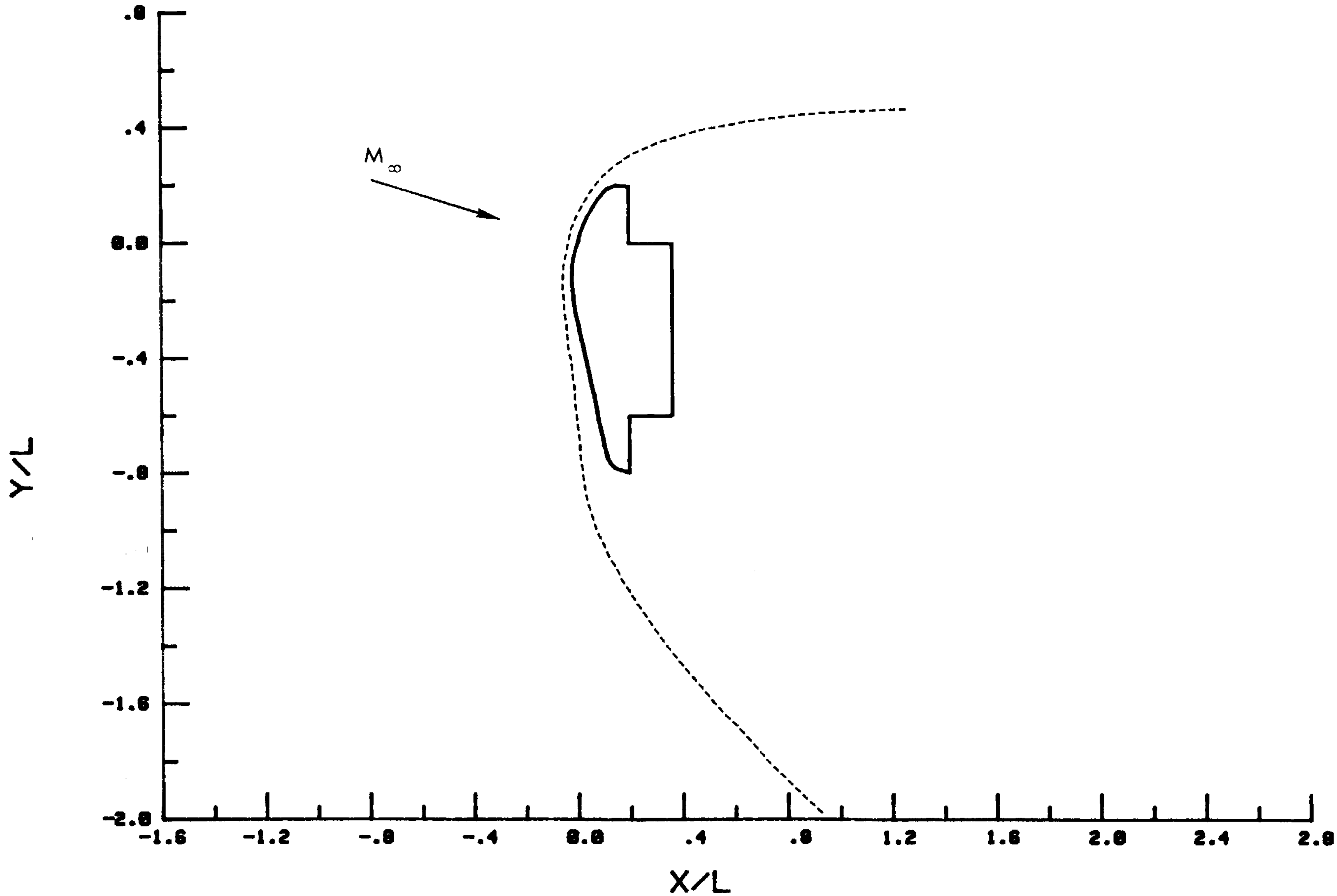

(c) $\alpha = 0°$.

Figure 12.- Continued.

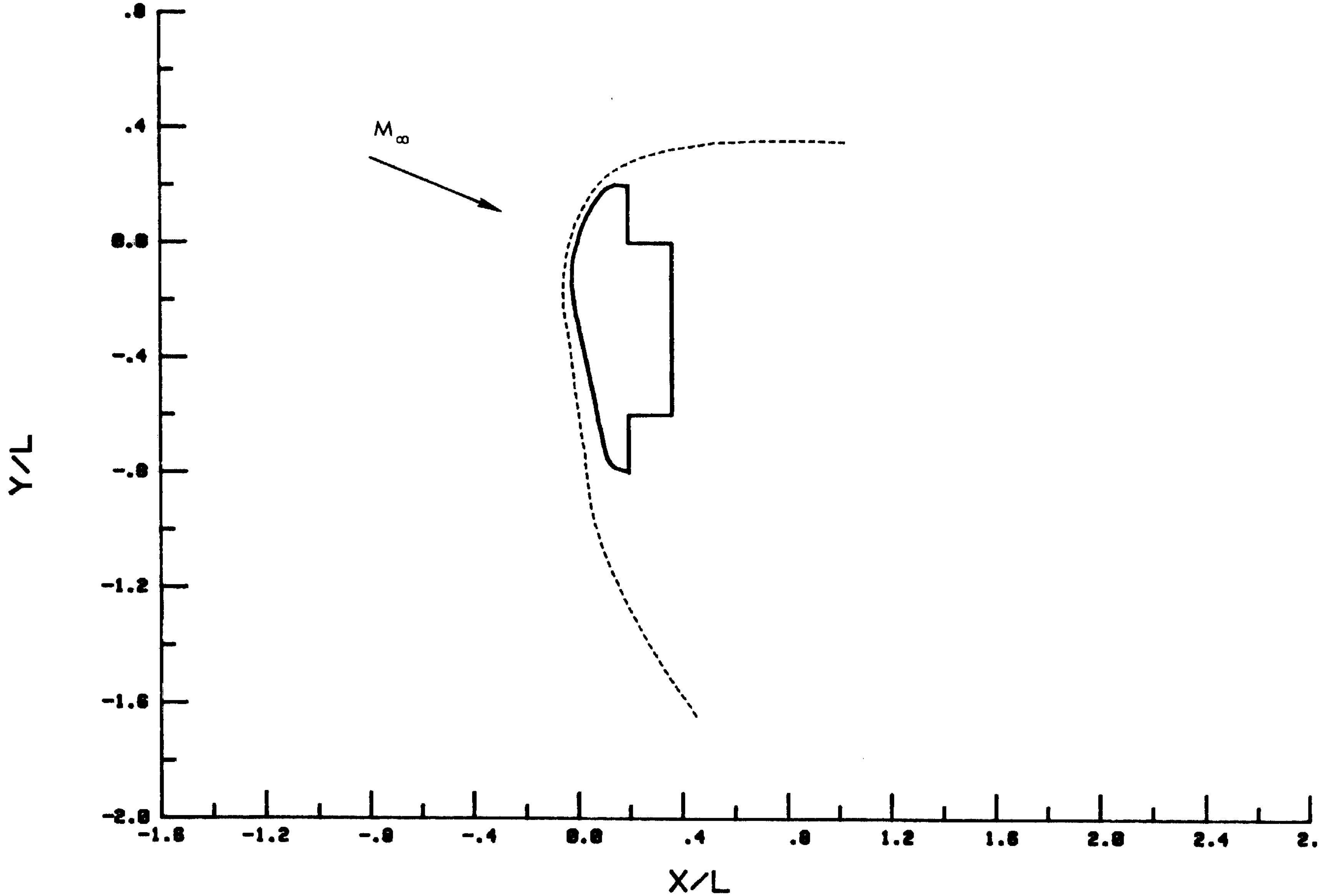

(d) $\alpha = -5°$.

Figure 12.- Continued.

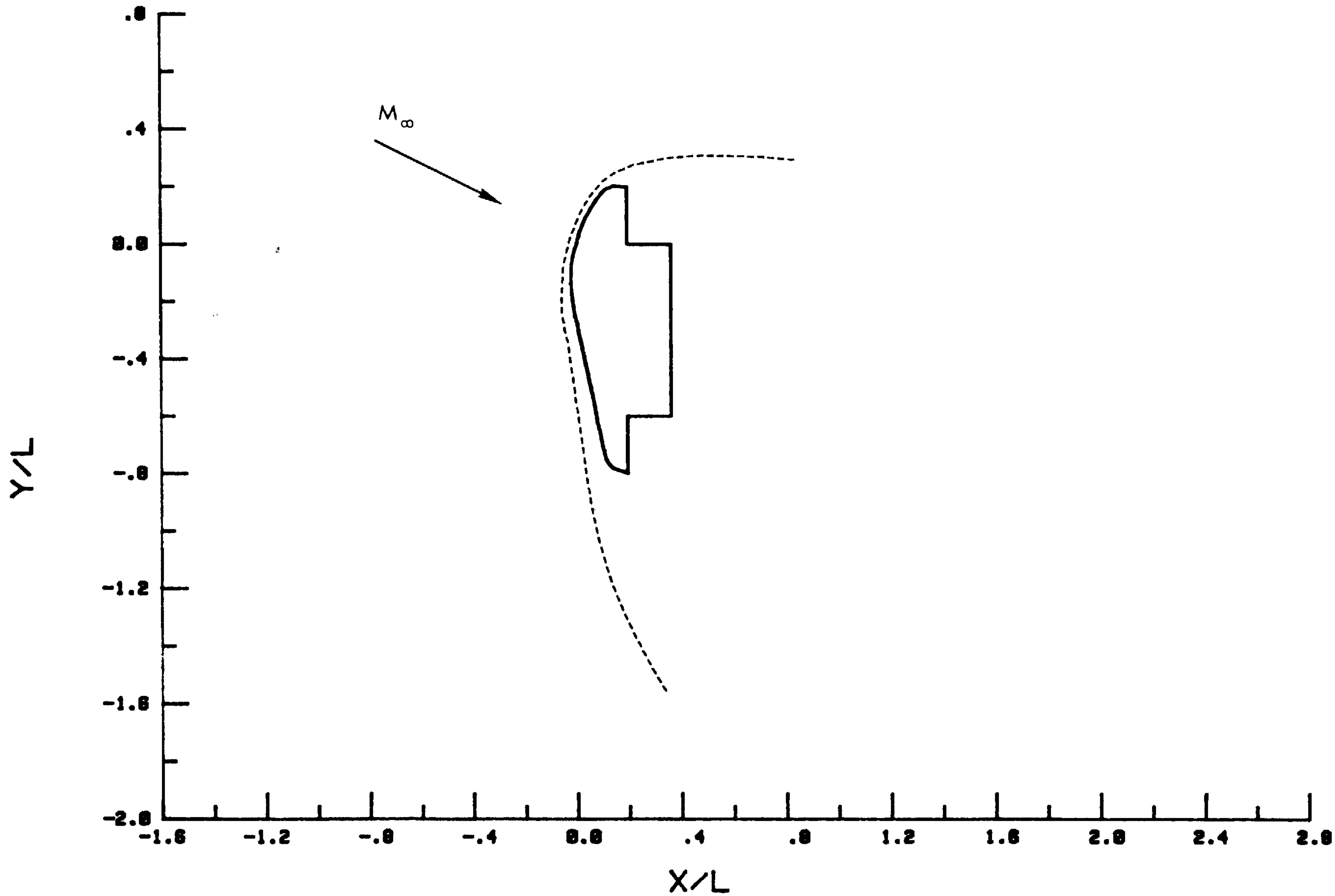

(e) $\alpha = -10°$.

Figure 12.- Concluded.

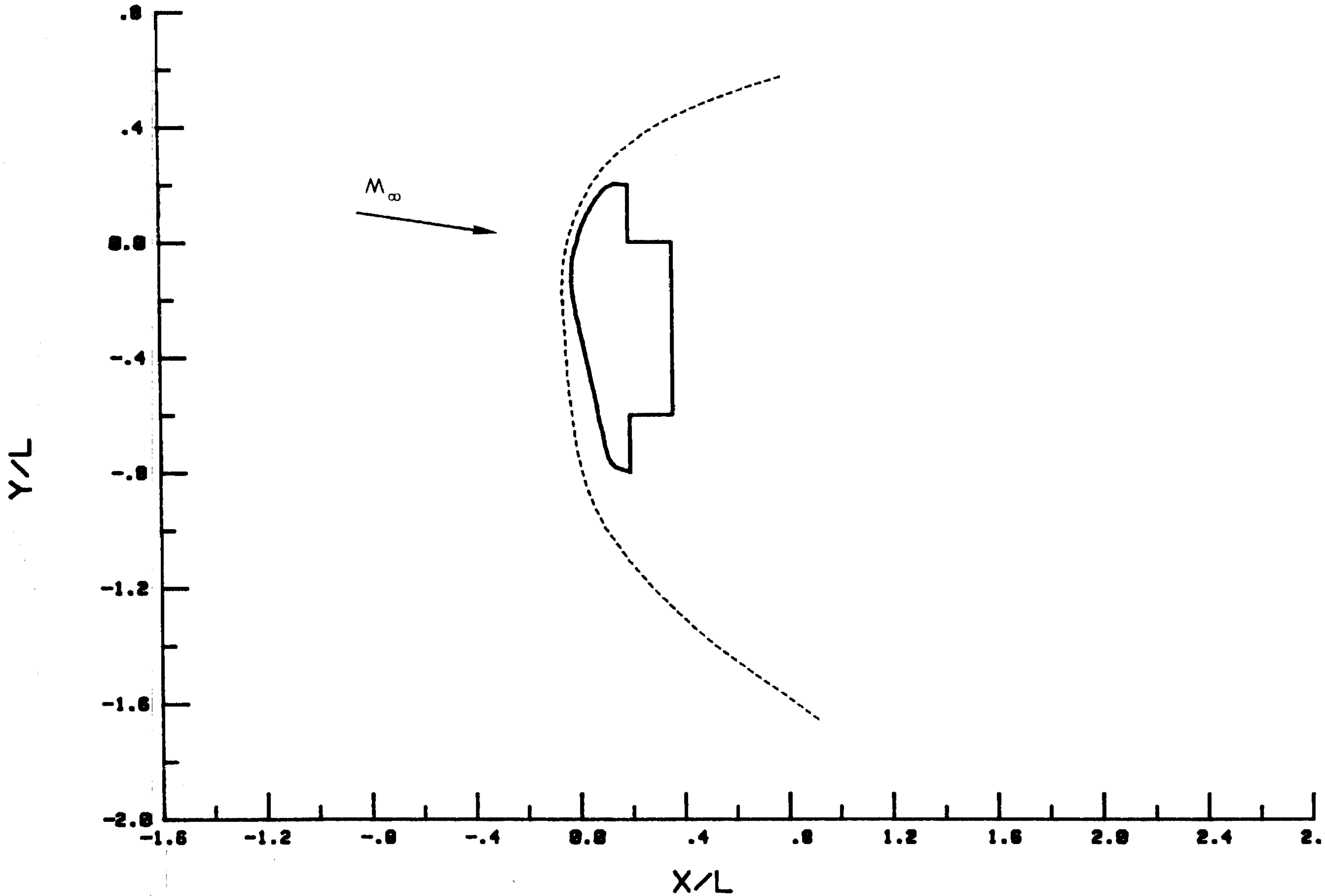

(a) α = 10°.

Figure 13.- Measured AFE shock shape in M_∞ = 6 CF_4 at $N_{Re,\infty}$ = 0.3 x 10^6/ft.

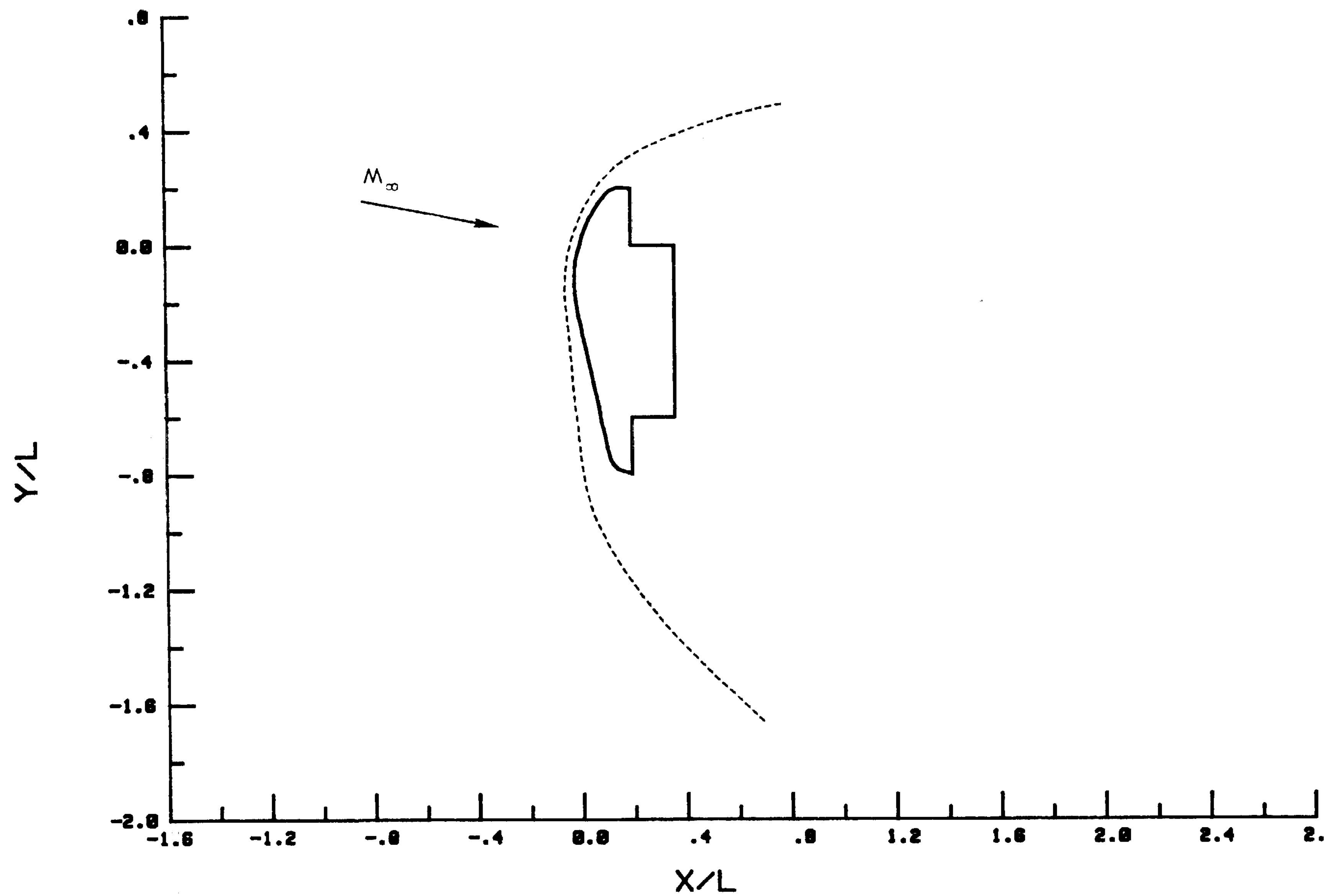

(b) α = 5°.

Figure 13.- Continued.

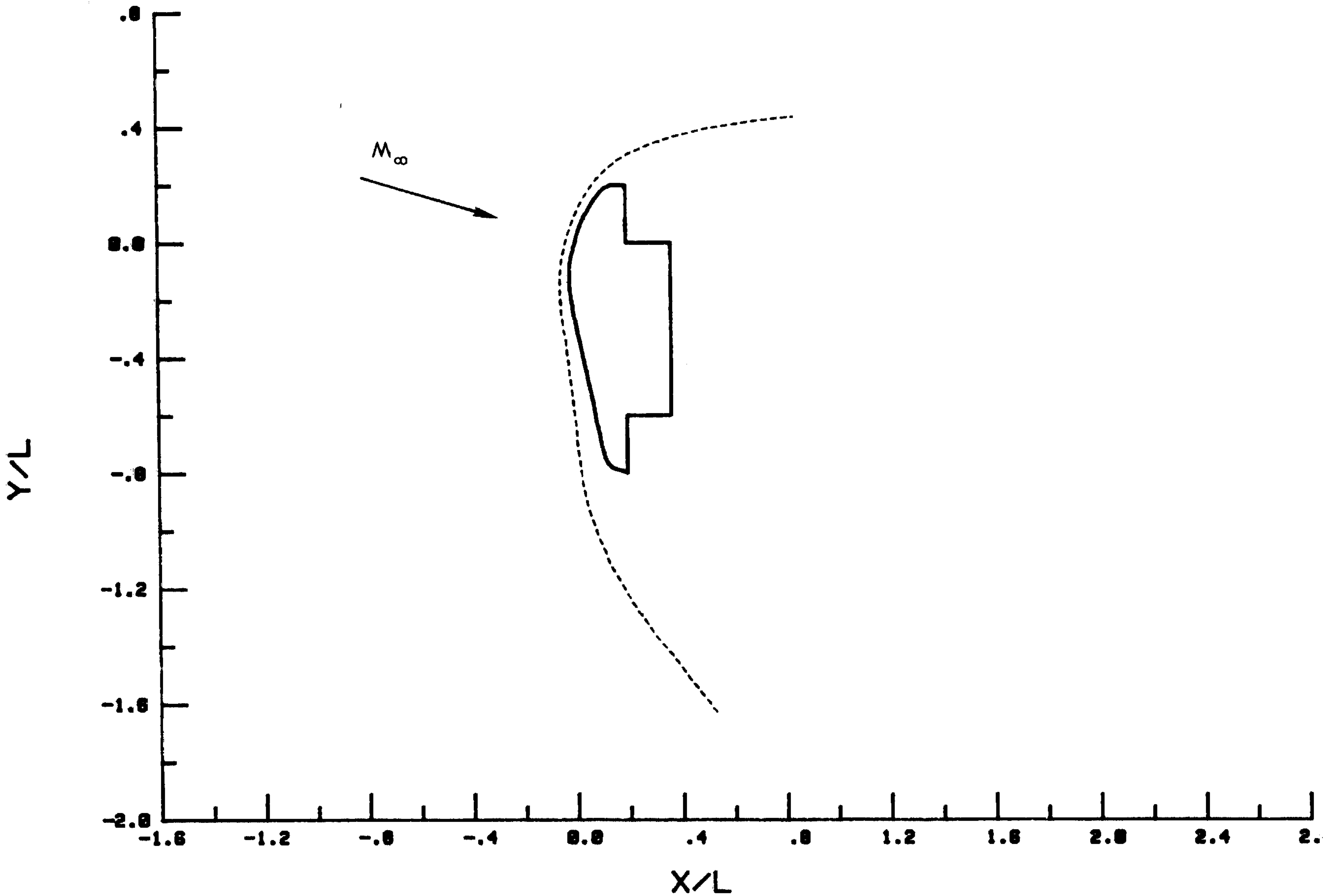

(c) $\alpha = 0°$.

Figure 13.- Continued.

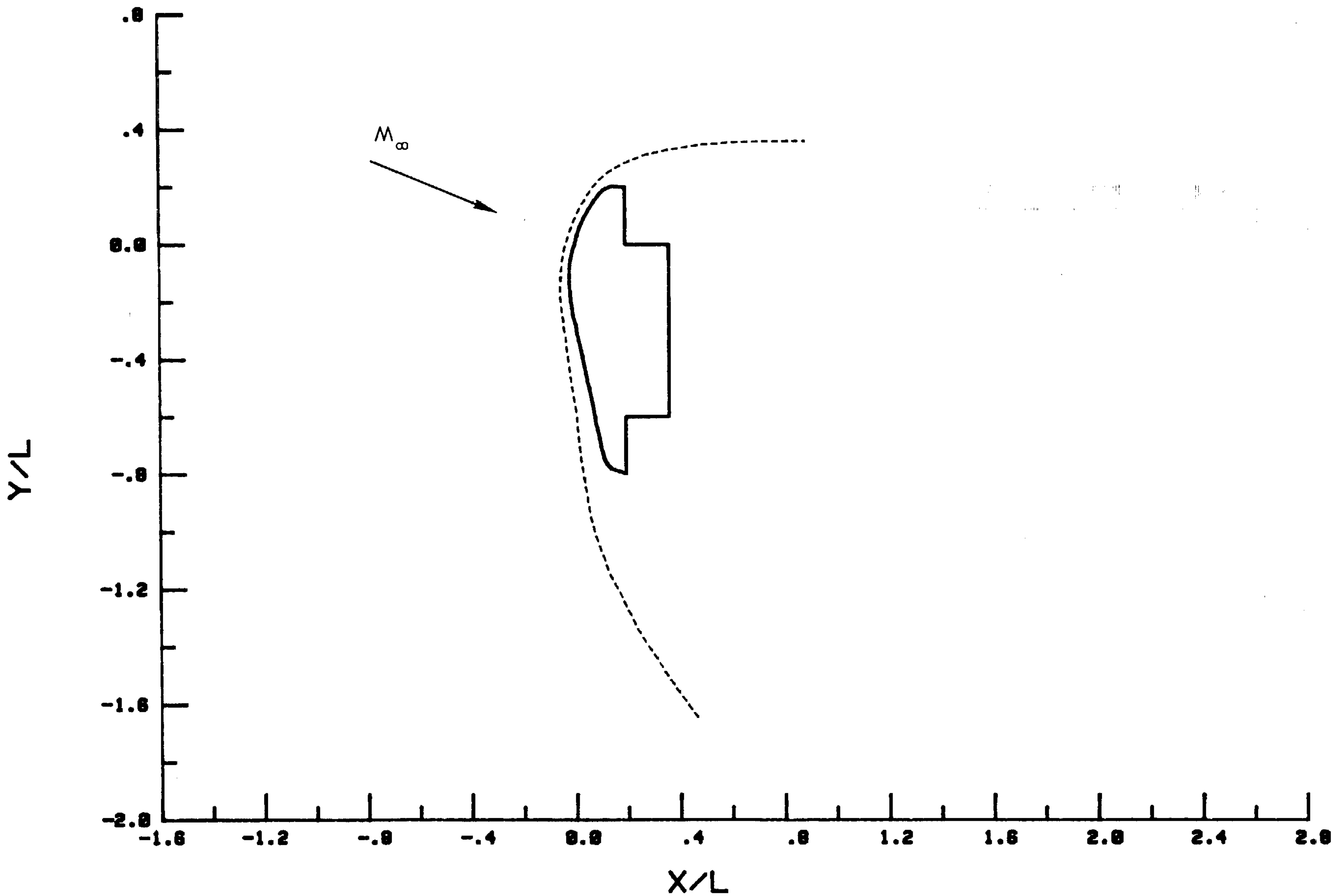

(d) $\alpha = -5°$.

Figure 13.- Continued.

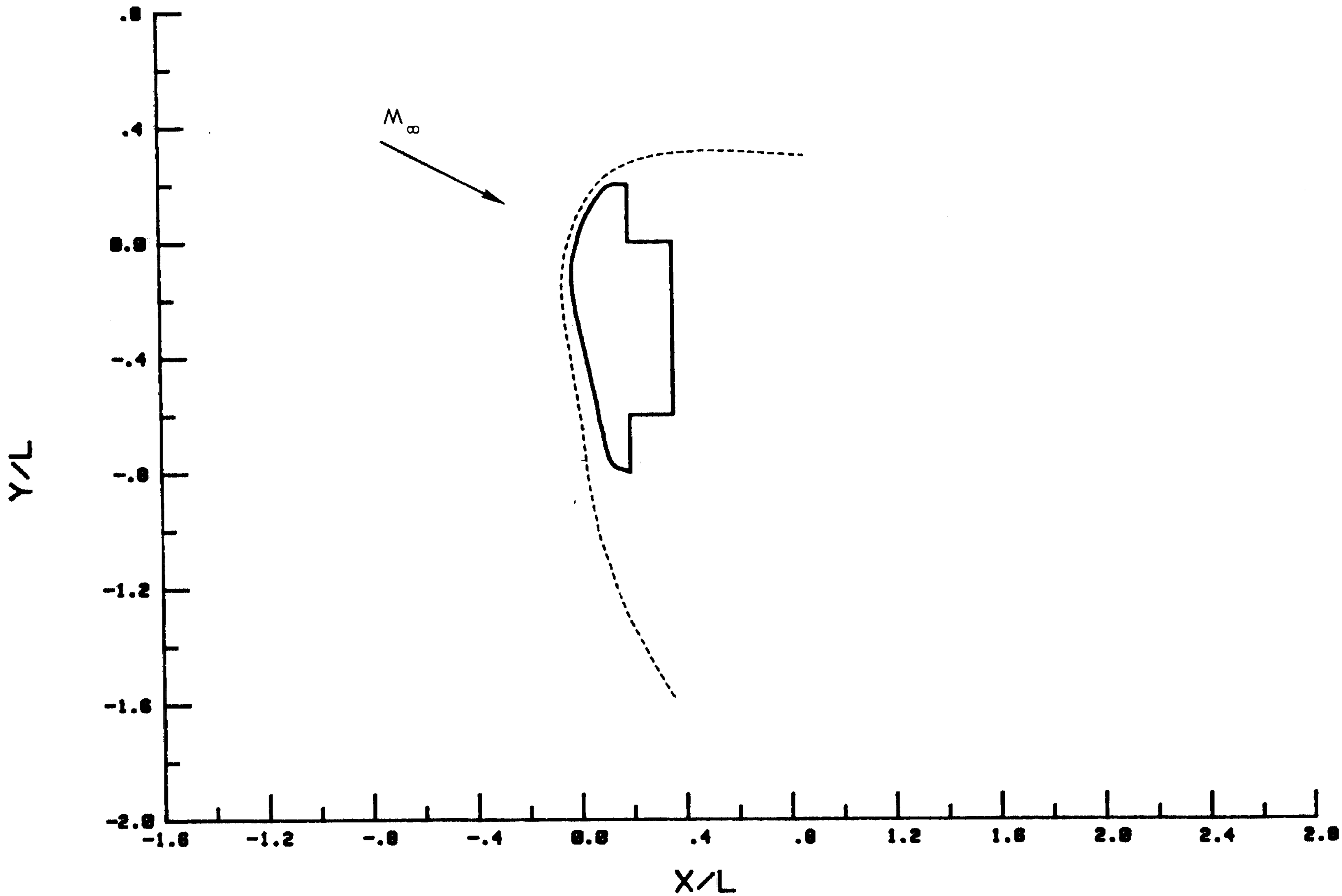

(e) α = -10°.

Figure 13.- Concluded.

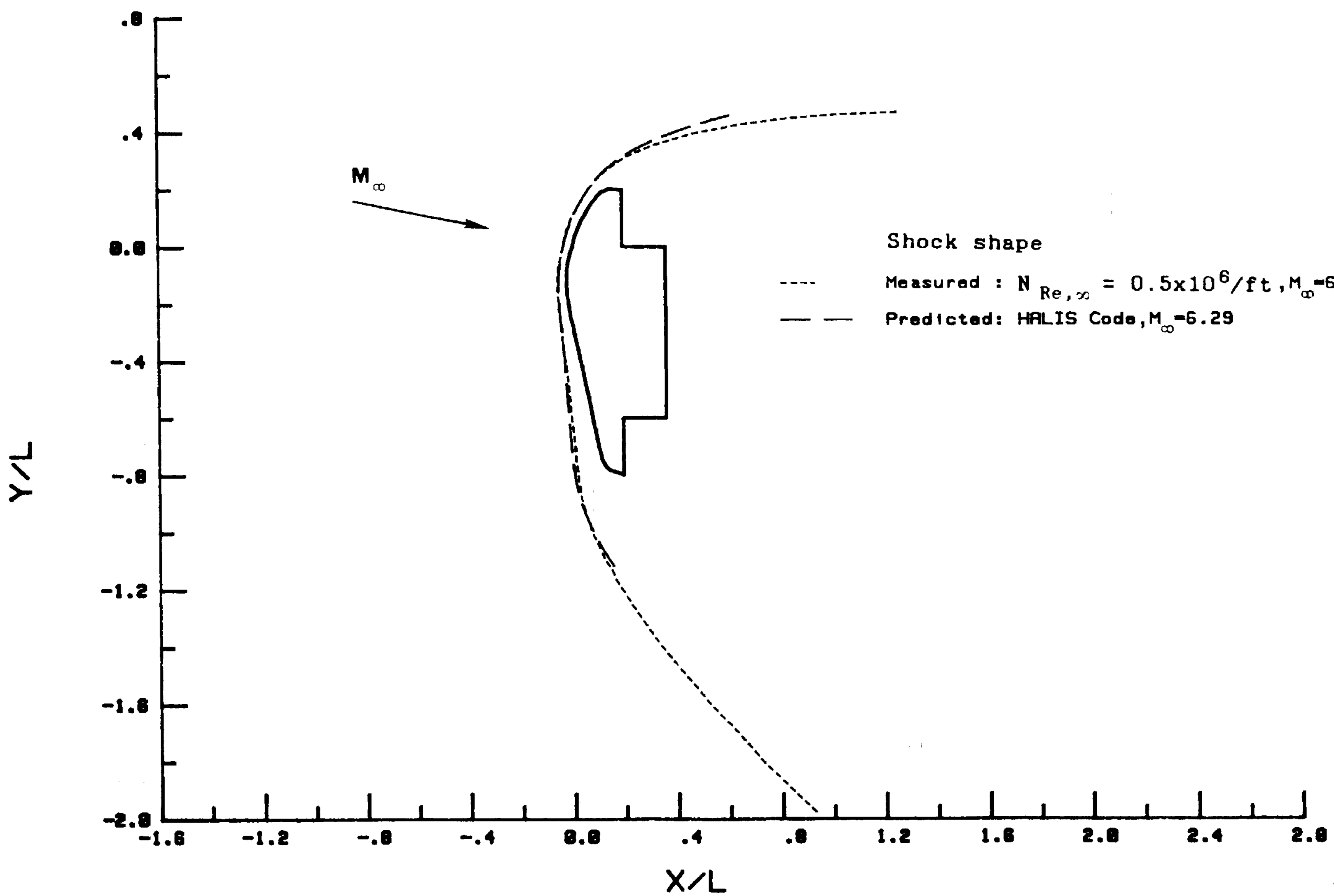

(a) $\alpha = 5°$.

Figure 14.- Comparison of predicted and measured shock shapes in CF_4.

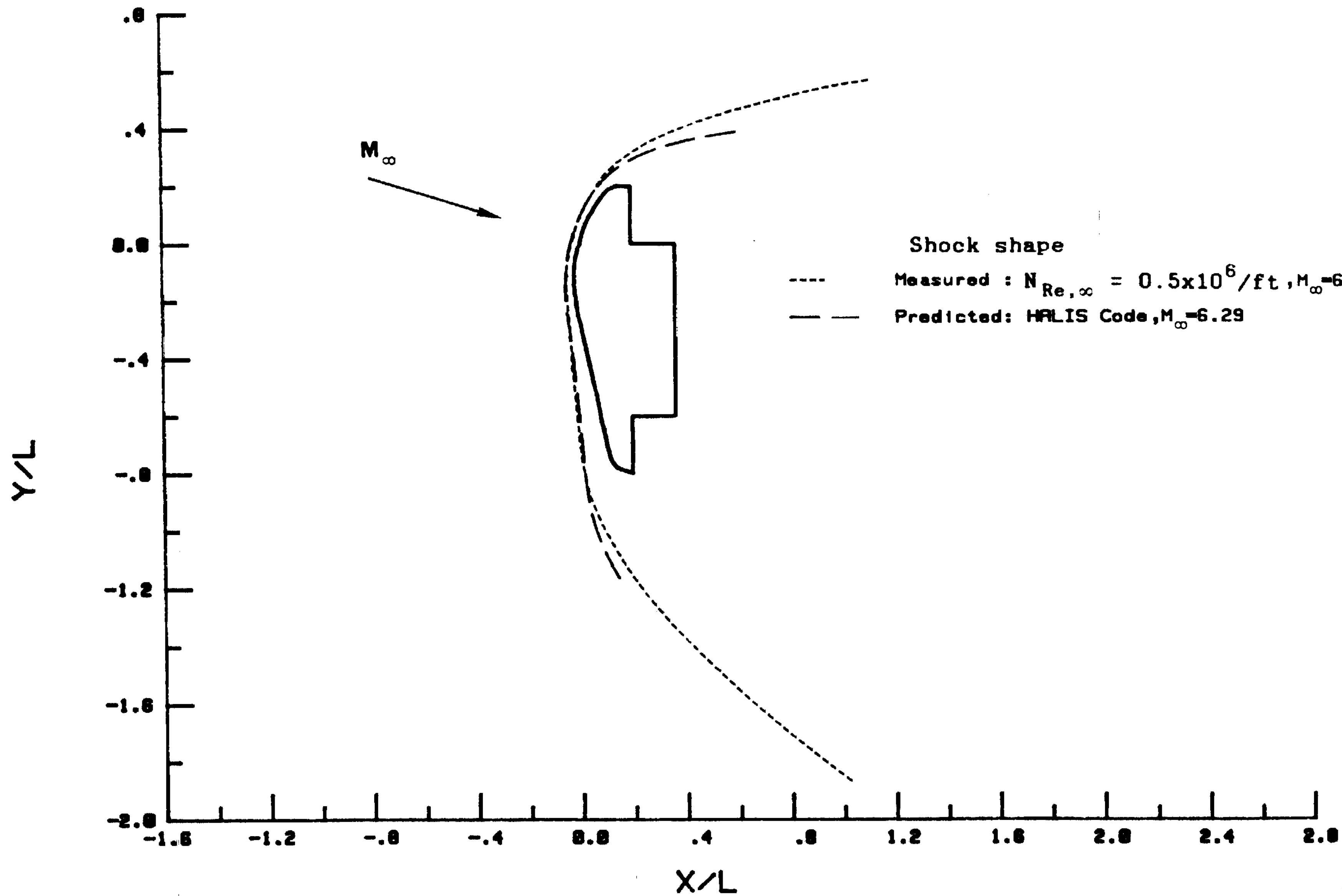

(b) $\alpha = 0°$.

Figure 14.- Concluded.

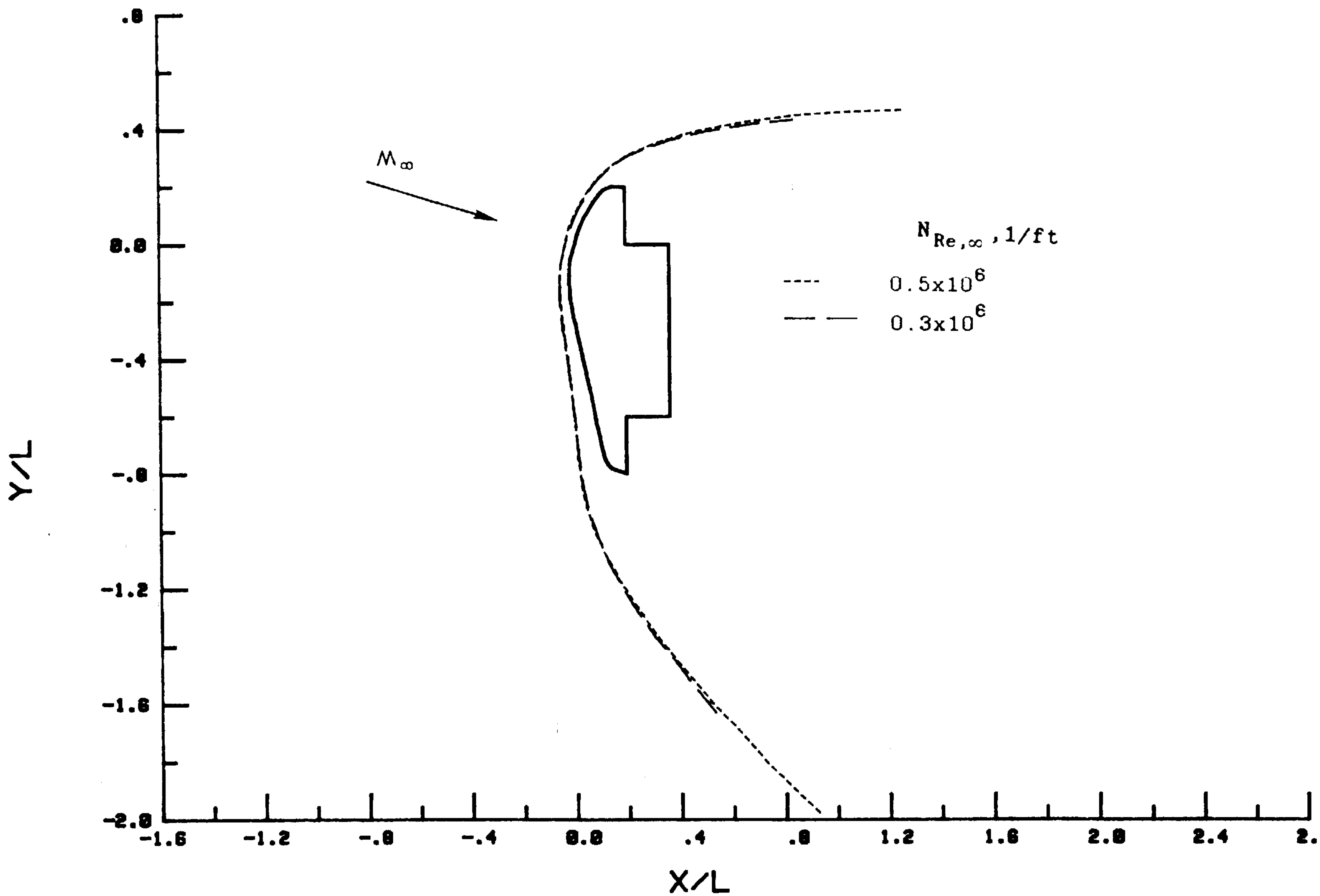

Figure 15.- Effect of $N_{Re,\infty}$ for $\alpha = 0°$ in $M_\infty = 6$ CF_4.

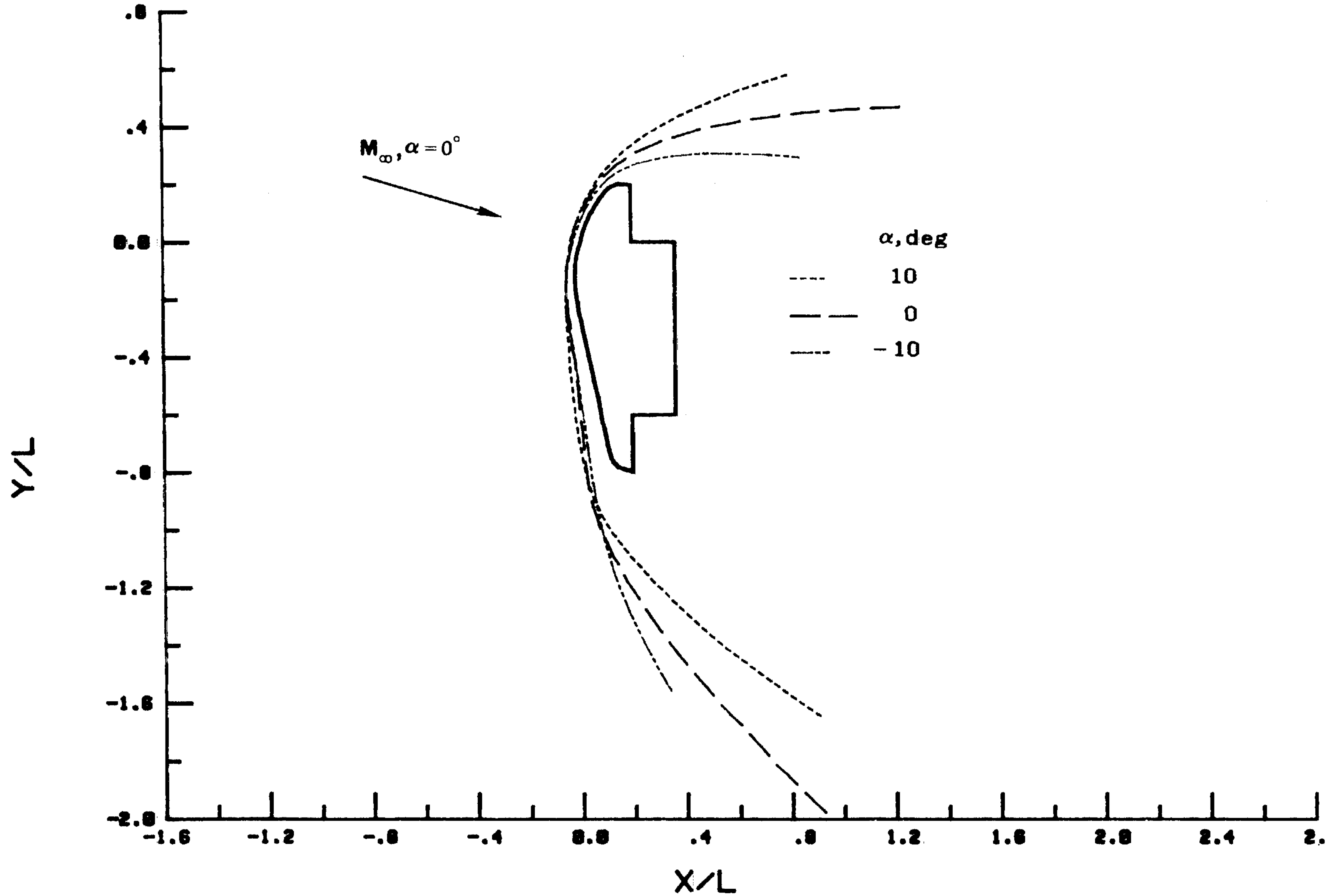

Figure 16.- Effect of α in $M_\infty = 6$ CF_4.

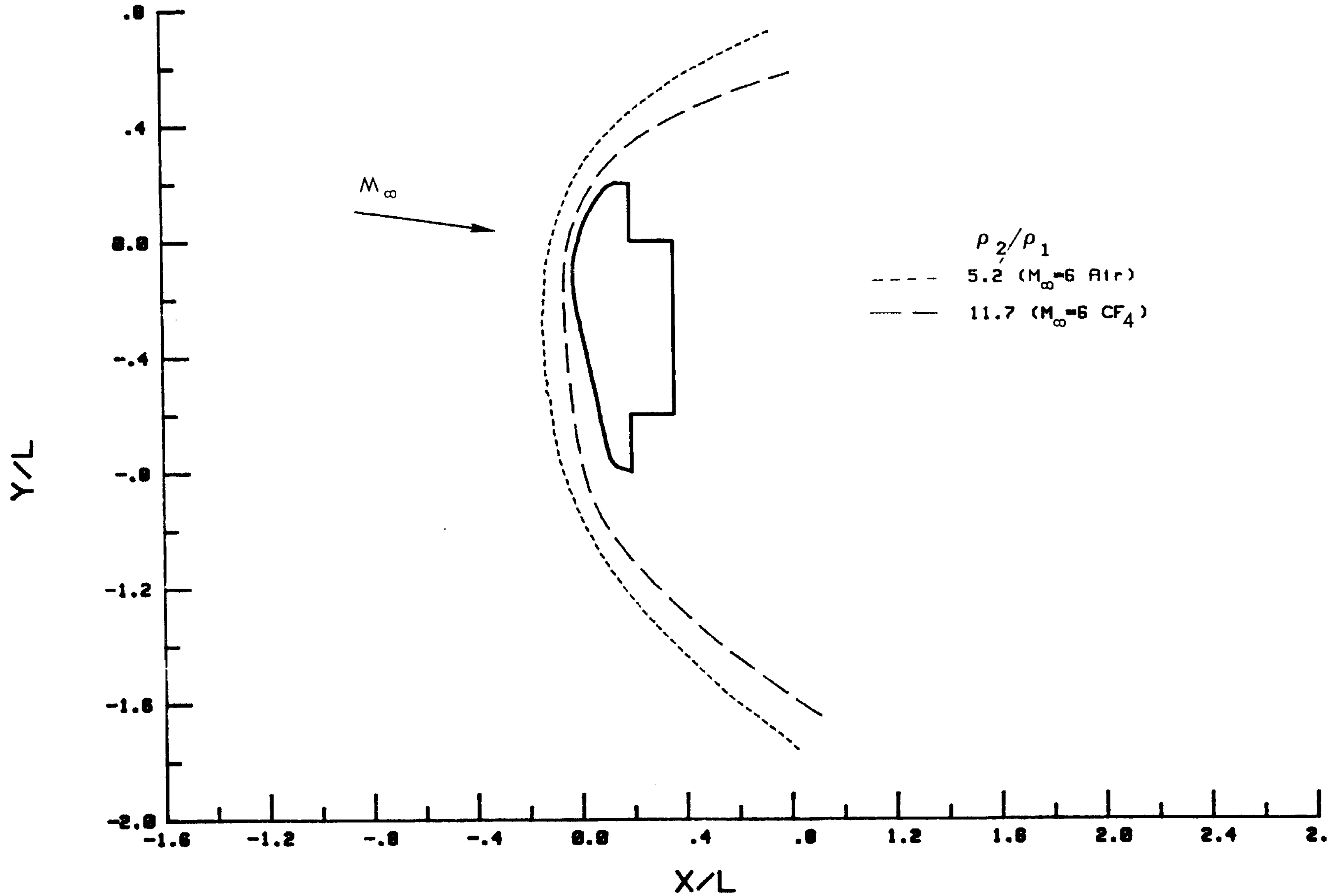

(a) α = 10°.

Figure 17.- Effect of ρ_2/ρ_1.

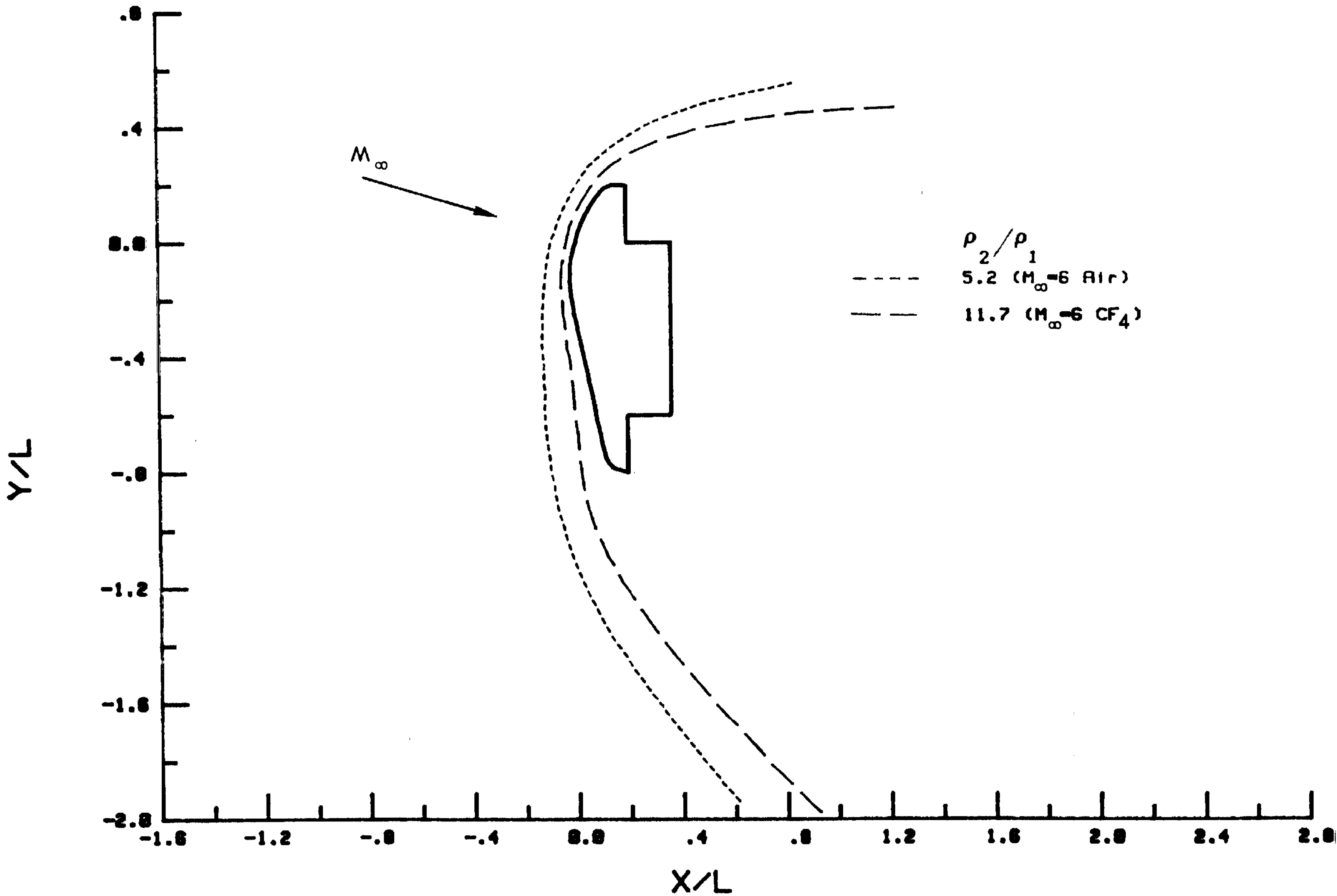

(b) α = 0°.

Figure 17.- Continued.

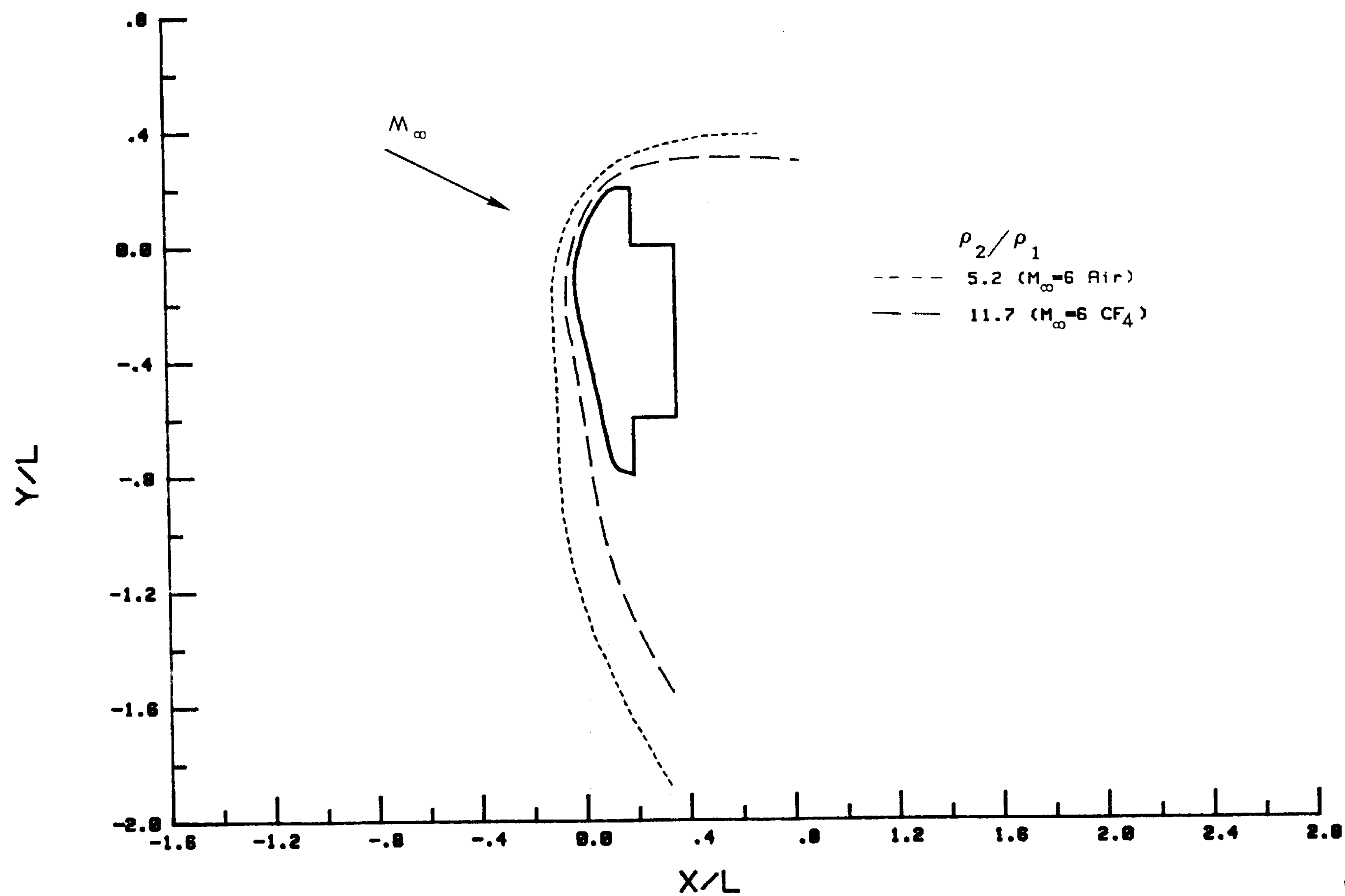

(c) α = -10°.

Figure 17.- Concluded.

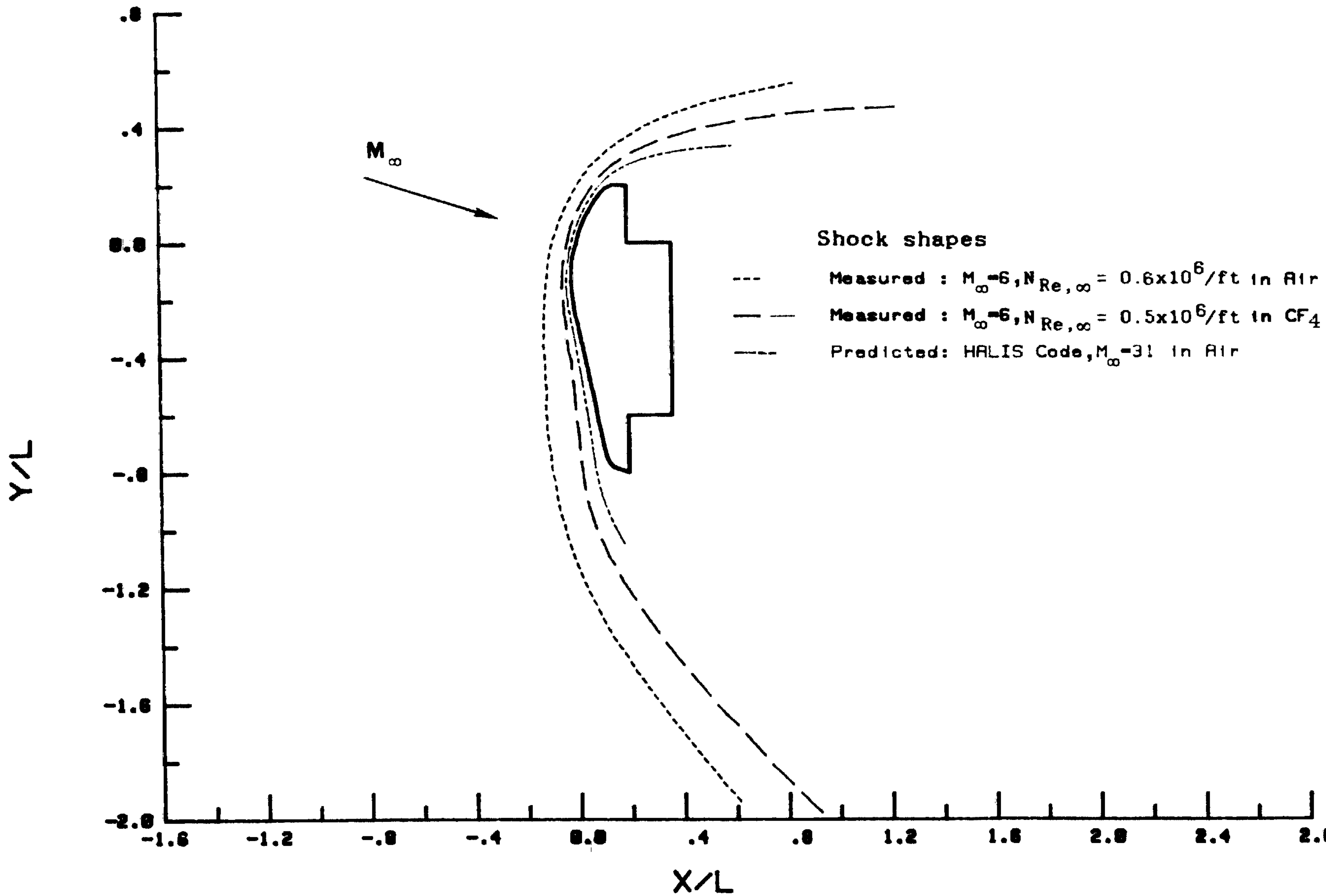

Figure 18.- Comparison of predicted flight and wind-tunnel-measured shock shapes for $\alpha = 0°$.

NASA
National Aeronautics and Space Administration

Report Documentation Page

1. Report No. NASA TM-100660	2. Government Accession No.	3. Recipient's Catalog No.

4. Title and Subtitle

Measured and Predicted Shock Shapes for AFE Configuration at Mach 6 in Air and in CF_4

5. Report Date

October 1988

6. Performing Organization Code

7. Author(s)

William L. Wells
and
Alan M. Franks

8. Performing Organization Report No.

10. Work Unit No.

583-01-11-02

9. Performing Organization Name and Address

Langley Research Center
Hampton, VA 23665-5225

11. Contract or Grant No.

13. Type of Report and Period Covered

Technical Memorandum

12. Sponsoring Agency Name and Address

National Aeronautics and Space Administration
Washington, DC 20546-0001

14. Sponsoring Agency Code

15. Supplementary Notes

16. Abstract

Shock shapes and stand-off distances were obtained for the Aeroassist Flight Experiment configuration from Mach 6 tests in air and in CF_4. Results were plotted for an angle-of-attack range from -10° to 10° and comparisons were made at selected angles with inviscid-flow predictions. Tests were performed in the LaRC 20-Inch Mach 6 Tunnel (air) at unit free-stream Reynolds numbers ($N_{Re,\infty}$) of 2×10^6/ft and 0.6×10^6/ft and in the LaRC Hypersonic CF_4 Tunnel at $N_{Re,\infty} = 0.5 \times 10^6$/ft and 0.3×10^6/ft. Within the range of these tests, $N_{Re,\infty}$ did not affect the shock shape or stand-off distance, and the predictions were in good agreement with the measurements. The shock stand-off distance in CF_4 was approximately one-half that in air. This effect resulted from the difference in density ratio across the normal shock, which was approximately 12 in CF_4 and 5 in air. In both test gases, the shock lay progressively closer to the body as angle of attack decreased.

17. Key Words (Suggested by Author(s))

shock shapes
hypersonic flow
Aeroassist Flight Experiment

18. Distribution Statement

[redacted]
until October 31, 1990
Subject Category 34

19. Security Classif. (of this report)	20. Security Classif. (of this page)	21. No. of pages	22. Price
Unclassified	Unclassified	55	

[redacted]